from hPSCs. We found that the HBCs derived from hPSCs can be maintained and proliferated on human laminin-111 (LN111)-coated dishes. To demonstrate that expandable, multipotent, and safe (i.e., devoid of residual undifferentiated cells) hPSC-derived HBCs could be maintained under our culture condition, the hPSC-derived HBCs were used for hepatic and biliary differentiation, colony assay, and transplantation into immunodeficient mice.

RESULTS

Human PSC-Derived Hepatoblast-like Cells Could Adhere onto Human LN111 via Integrin α6 and β1

The HBCs were generated from hPSCs (hESCs and hiPSCs) as described in Figure 1A (details of the characterization of hPSC-derived HBCs are described in Figure 3). Definitive endoderm differentiation of hPSCs was promoted by stage-specific transient transduction of FOXA2 in addition to the treatment with appropriate soluble factors (such as Activin A). Overexpression of FOXA2 is not necessary for establishing the hPSC-derived HBCs, but it is helpful for efficient generation of the hPSC-derived HBCs. On day 9, these hESC-derived populations contained two cell populations with distinct morphology (Figure 1B). One population resembled human hepatic stem cells that were isolated from human fetal liver (shown in red) (Schmelzer et al., 2007), whereas the other population resembled definitive endoderm cells (shown in green) (Hay et al., 2008). The population that resembled human hepatic stem cells was alpha-1-fetoprotein (AFP) positive, whereas the other population was AFP negative (Figure 1C, left). On day 9, the percentage of AFP-positive cells was approximately 80% (Figure 1C, right). To characterize these two cell populations (hESC-derived HBC and non-HBC [NHBC] populations), the colonies were manually isolated by using a pipette, and then the gene expression analysis was performed. The gene expression levels of *AFP*, *CD133*, *EpCAM*, *CK8*, and *CK18* in the hESC-derived HBCs were higher than those in the bulk population containing both hESC-derived HBCs and NHBCs (*CD133*, *EpCAM*, *CK8*, and *CK18* were named as pan-hepatoblast markers and are known to be strongly expressed in both human hepatic stem cells and hepatoblasts [Schmelzer et al., 2007; Zhang et al., 2008]) (Figure 1D). On the other hand, the gene expressions of *AFP*, *CD133*, *EpCAM*, *CK8*, and *CK18* in the hESC-derived NHBCs were hardly detected. The gene expression levels of DE, mesendoderm, and pluripotent markers in the hESC-derived NHBCs were higher than those in the hESC-derived HBCs, indicating that the hESC-derived NHBCs could remain in a more undifferentiated state than the hESC-derived HBCs (Figures S1A–S1C available online). These results suggest that hepatoblast-like cells could be differentiated from hPSCs.

To purify the hESC-derived HBCs, these cells were plated onto dishes coated with various laminins. There are 15 different laminin isoforms in human tissues. Although laminin is known to be useful to sustain mouse hepatoblasts (Tanimizu et al., 2004), it remains unknown which human laminin isoform has the potential to purify and expand the HBCs. To identify a human laminin isoform that would be useful for purifying hESC-HBCs, the hESC-HBCs and -NHBCs were plated onto dishes coated with various types of commercially available human laminins (Figure 1E). The hESC-derived HBCs could more efficiently adhere onto the human LN111-coated dish compared with hESC-derived NHBCs or unseparated populations (containing both HBCs and NBCs). These data suggest that a hESC-derived HBC population can be purified from the unseparated populations by culturing on human LN111-coated dishes. Because integrins are known to be important molecules for cell adhesion to the ECM including laminins, we expected that certain types of integrins would allow selective adhesion of the hESC-derived HBCs to human LN111-coated dish. The gene expression levels of various integrins were examined (Figure 1F). Among the integrin α subunits, the gene expression level of *integrin α6* in the hESC-derived HBCs was significantly higher than that in the hESC-derived NHBCs. In contrast, among the integrin β subunits, the gene expression level of *integrin β1* was higher than those of *integrin β2* and *β3* in all cell populations. The hESC-derived HBCs, but not NHBCs, expressed both integrin α6 and β1 (Figure S1D). Almost all adhesion of the hESC-derived HBCs to a human LN111-coated dish was inhibited by both function-blocking antibodies to integrin α6 and β1 (Figure 1G). These results indicated that the hESC-derived HBCs could attach to a human LN111-coated dish via integrin α6 and β1.

The hPSC-Derived HBCs Could Be Proliferated and Maintained on a Human LN111-Coated Dish

To obtain the purified hESC-derived HBC population, the hESC-derived cells (day 9) were plated onto a human LN111-coated dish, and then unattached cells were removed at 15 min after plating (Figure 2A). Among various laminins, only human LN111 could proliferate (Figure 2B) and purify (Figure 2C) the AFP-positive population in the presence of HGF and EGF. During culture on the human LN111-coated dish, the morphology of the hESC-derived HBCs gradually changed into that of human hepatoblasts (Figure S1E) (Schmelzer et al., 2007). Therefore, the characteristics of hESC-derived HBCs might be changed by culturing on a human LN111-coated dish (details of the characterization of the hESC-derived HBCs are described in Figure 3). After culturing on a human LN111-coated

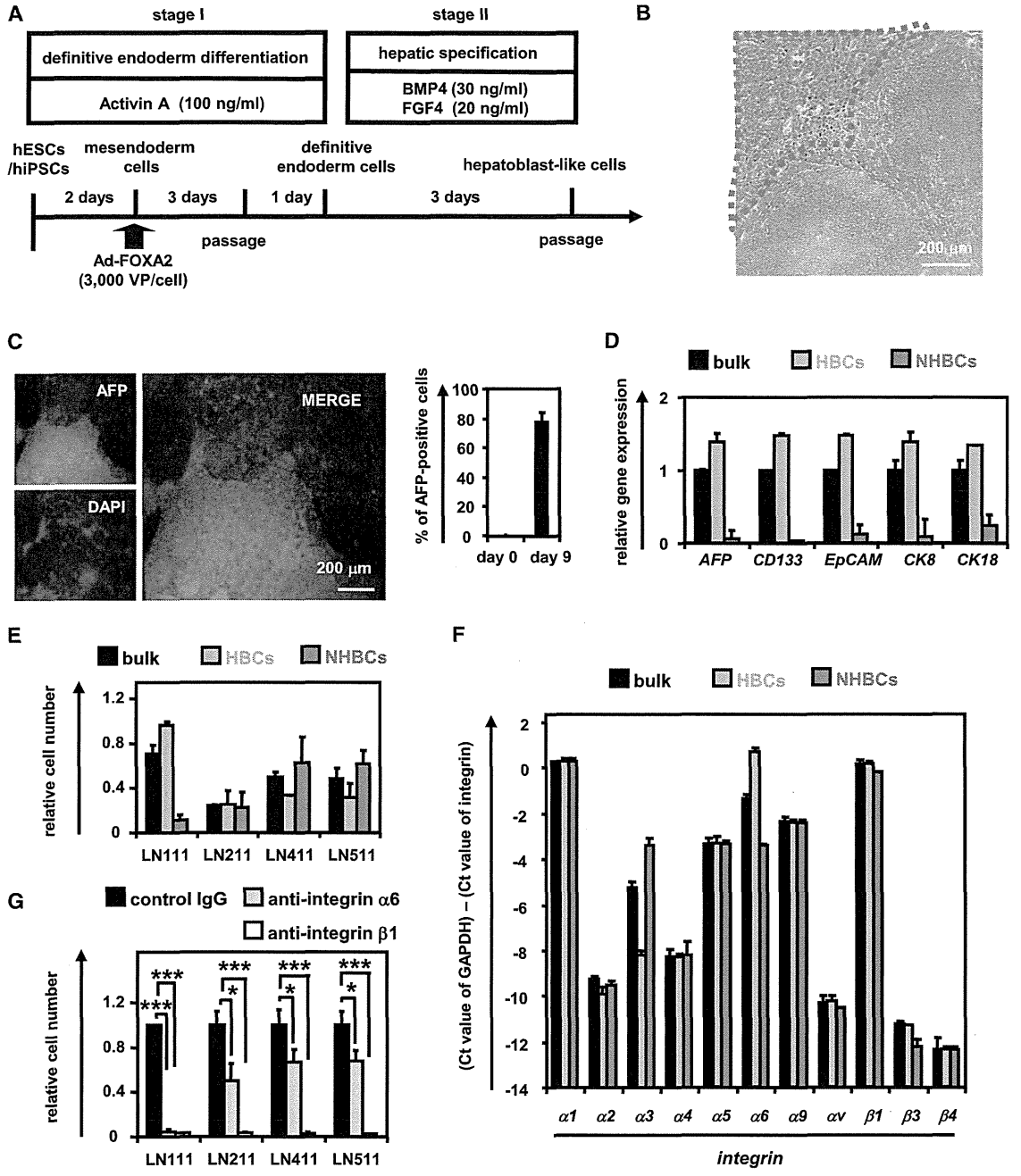

Figure 1. The Human ESC-Derived HBCs Selectively Attached to a Human LN111-Coated Dish via Integrin α6 and β1

(A) The procedure for the differentiation of hESCs (H9) into hepatoblast-like cells (HBCs) is presented schematically. Details are described in the Experimental Procedures.

(B) Phase-contrast micrographs of the hESC-derived HBCs (red) and non-HBCs (NHBCs) (green) are shown.

(C) The hESC-derived cells (day 9) were subjected to immunostaining with anti-AFP (red) antibodies. The percentage of AFP-positive cells was examined on day 0 or 9 by using FACS analysis. Data represent the mean ± SD from ten independent experiments. Cells on "day 0" and "day 9" were compared using Student's t test ($p < 0.01$).

(D) On day 9, the hESC-derived HBCs and NHBCs were manually picked, and the gene expression levels of *AFP* and pan-hepatoblast markers (*CD133*, *EpCAM*, *CK8*, and *CK18*) were measured by real-time RT-PCR. The gene expression levels of *AFP* and pan-hepatoblast markers in the hESC-derived cells (day 9; bulk) were taken as 1.0. Data represent the mean ± SD from four independent experiments. The gene expression levels in the HBCs were significantly different among the three groups (bulk, HBCs, and NHBCs) based on analysis with one-way ANOVA followed by Bonferroni post hoc tests ($p < 0.05$).

(legend continued on next page)

dish for a week, almost all of the cells were still AFP positive (Figures 2C and 2D). To characterize the cells cultured on various types of human laminins for 7 days, the gene expression levels of *AFP* and pan-hepatoblast (*CD133*, *CK8*, *CK18*, and *EpCAM*) markers were examined on day 16 (Figure 2E). The gene expression levels of *AFP* and pan-hepatoblast markers in the hESC-derived HBCs P1 (HBCs passaged once) did not change as compared with those of the hESC-derived HBCs (day 9; HBC P0) (the definitions of HBC P0, P1, P10, and clone in the present study are shown in Figure S3). The gene expression levels of mature hepatocyte and cholangiocyte markers in the hESC-derived HBC P1 did not change as compared with those of the hESC-derived HBC P0 (day 9) (Figure S1F). These results suggest that the characteristics of the hESC-derived HBC P1 are similar to those of the hESC-derived HBC P0, although their morphologies are quite different from each other. Interestingly, the gene expression levels of mature cholangiocyte markers in the cells cultured on human LN411- or 511-coated dishes were upregulated as compared with those of the hESC-derived HBC P0 (day 9) (Figure S1F), suggesting that human LN411 and 511 might promote biliary differentiation. Importantly, both hESC-derived HBCs and hiPSC-derived HBCs could extensively proliferate on a human LN111-coated dish for more than 15 passages (Figure 2F) in the presence of HGF and EGF. Doubling times of hESC (H9)-derived HBCs and hiPSC (Dotcom)-derived HBCs were approximately 78 and 67 hr, respectively. Almost all of the populations cultured on a human LN111-coated dish were AFP positive (Figure 2G). Taken together, these results suggested that the hPSC-derived HBCs would proliferate and be maintained on a human LN111-coated dish.

Characterization of the hESC-Derived HBCs

To characterize the hESC-derived HBCs, the gene expression profiles in the hESC-derived purified HBCs (HBC P0), short-term cultured HBCs (HBCs passaged once [HBC P1]), and long-term cultured HBC (HBCs passaged ten times [HBC P10]) were examined. The hESC-derived HBCs were AFP positive (Figure 3A). Although the hESC-derived HBC P0 were negative for ALB, CK7, and CK19, the hESC-derived HBC P1 and P10 were positive for these genes (Figure 3A). Both integrin α6 and β1 (receptors of LN111) were strongly expressed in the hESC-derived HBC P0, P1, and P10 (Figure 3B). The gene expression levels of human hepatic stem cell markers (*N-CAM* and *Claudin 3* [Schmelzer et al., 2007]; these are not expressed in human hepatoblasts) in the hESC-derived HBC P0 were higher than those of the hESC-derived HBC P1 and P10 (Figure 3C). However, the gene expression level of *CK19* in the hESC-derived HBC P0 was lower than that of the hESC-derived HBC P1 and P10. The gene expression levels of pan-hepatoblast markers in the hESC-derived HBC P0 were similar to those of the hESC-derived HBC P1 and P10 (Figure 3D). The gene expression levels of human hepatoblast markers (*ALB*, *CYP3A7*, and *I-CAM* (Schmelzer et al., 2007), none of which were expressed in human hepatic stem cells) in the hESC-derived HBC P1 and P10 were higher than those of the hESC-derived HBC P0 (Figure 3E). However, the AFP expression level in the hESC-derived HBC P0 was similar to that of the hESC-derived HBC P1 and P10. Because the gene expression levels of mature hepatocyte and cholangiocyte markers in the hESC-derived HBC P1 and P10 were not increased as compared with those in the hESC-derived HBC P0 (Figure 3F), the hESC-derived HBC P1 and P10 were not segregated into either of the hepatic and biliary lineages. We also examined the gene expression levels of hepatoblast markers, which have been reported only in mice and not in humans (Figure 3G). The characteristics of the hPSC-derived HBCs are summarized in Figure S3. In addition, hESC-derived HBC P0 and HBC P10 showed normal karyotypes (Figure S2A). Therefore, the genetic stability of the HBCs was confirmed throughout the maintenance period. Taken together, these results suggest that the hESC-derived HBC P0 resemble human hepatic stem cells and the hESC-derived HBC P1 and P10 resemble human hepatoblasts, although some gene expression patterns in the hESC-derived HBCs differ from those in human hepatic stem cells and human hepatoblasts, respectively.

(E) The hESC-derived cells (day 9; bulk), HBCs, and NHBCs were plated onto human LN111-, 211-, 411-, or 511-coated dishes, and the attached cells were counted at 60 min after plating. The cell number that was initially plated was taken as 1.0. Data represent the mean ± SD from four independent experiments. The number of attached HBCs on LN111-coated dishes were significantly different among three groups (bulk, HBCs, and NHBCs) based on analysis with one-way ANOVA followed by Bonferroni post hoc tests ($p < 0.05$).

(F) The gene expression levels of the indicated integrins were measured in the hESC-derived cells (day 9; bulk), HBCs, and NHBCs by real-time RT-PCR. Data represent the mean ± SD from four independent experiments. The gene expression levels of *integrin α3* and *α6* in the HBCs were significantly different among three groups (bulk, HBCs, and NHBCs) based on analysis with one-way ANOVA followed by Bonferroni post hoc tests ($p < 0.05$).

(G) The adhesion of the hESC-derived HBCs to human LN111-, 211-, 411-, or 511-coated dishes was examined by using the indicated integrin antibodies. IgG antibodies were used as a control for uninhibited cell adhesion. The number of attached cells was estimated at 60 min after plating. The cell number in the control IgG-treated group was taken as 1.0. Data represent the mean ± SD from three independent experiments. "Control IgG" and "anti-integrin α6 or integrin β1" were compared using Student's t test. *$p < 0.05$; ***$p < 0.001$. See also Figure S1 and Tables S2–S5.

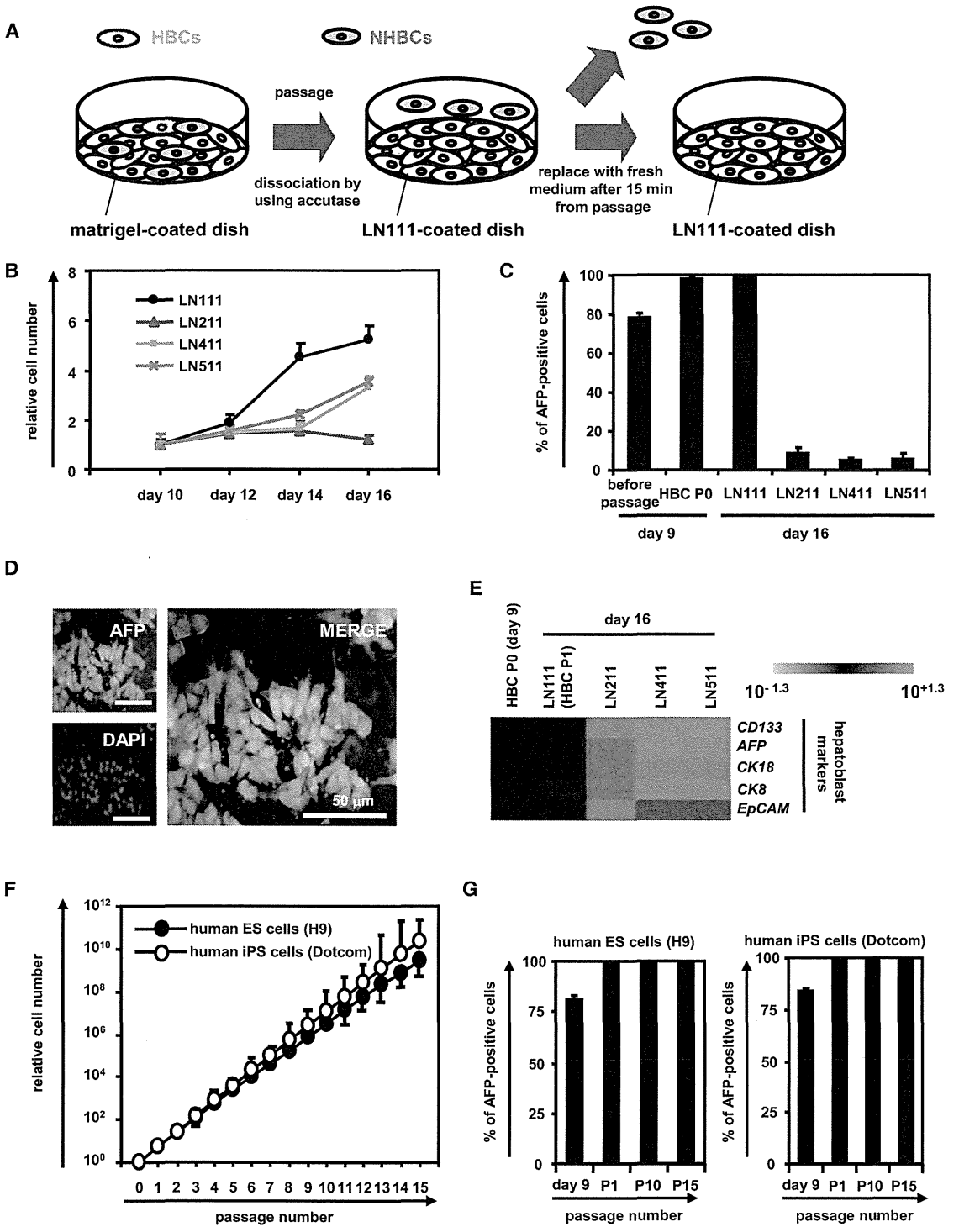

Figure 2. The hESC-Derived HBCs Could Be Proliferated and Maintained on a Human LN111-Coated Dish

(A) The hESC (H9)-derived cells (day 9) were plated onto a human LN111-coated dish. At 15 min after plating, the unattached cells were removed.

(B) The hESC (H9)-derived cells (day 9) were plated onto a human LN111, 211, 411, or 511-coated dish, and then the cell number were counted on days 10, 12, 14, and 16. The cell number on day 10 was taken as 1.0. Data represent the mean ± SD from three independent experiments. "LN111" was significantly different among four groups (LN111, 211, 411, and 511) on day 14 and 16 based on analysis with one-way ANOVA followed by Bonferroni post hoc tests ($p < 0.05$).

(legend continued on next page)

In order to examine whether the hESC-derived HBC P0 have the potential to proliferate clonally on various types of human laminins, single HBCs were plated on separate wells of a human LN111-coated 96-well plate at a low density (one cell per one well) (Table S1). Single cells that attached to the human LN111-coated dish were AFP positive and HNF4α positive (Figure S2B). At 7 days after plating, the hESC-derived HBC colonies (albumin [ALB]- and cytokeratin 7 [CK7] double positive) (a representative colony is shown in Figure S2C) were efficiently generated from the hESC-derived HBC P0 on a LN111-coated dish. Taken together, these results showed that the hESC-derived HBCs could be generated from both the hESC-derived HBC P0 population and the single hESC-derived HBC P0.

The hPSC-Derived HBCs Could Differentiate into Both Hepatic and Biliary Lineages In Vitro

To examine whether the hESC-derived HBCs have the potential to differentiate into both hepatic and biliary lineages, first, these cells were differentiated into hepatocyte-like cells as described in Figure 4A. After 2 weeks of hepatic differentiation, almost all of the cells were polygonal in shape (Figure 4B) and were CYP3A4, αAT, and ALB positive (Figure 4C). The gene expression levels of mature hepatocyte markers in the HBC P0-, HBC P10-, or HBC clone-derived hepatocyte-like cells were higher than those in the cells that had not undergone hepatic differentiation (Figure 4D), although the gene expression levels of mature cholangiocyte markers in these cells did not change (Figure 4E). The ASGR1-positive cells in the HBC P0-, HBC P10-, and HBC clone-derived population accounted for approximately 60%, 90%, and 90% of the total, respectively (Figure 4F). The HBC P0-, HBC P10-, or HBC clone-derived hepatocyte-like cells had the ability to produce ALB (Figure 4G, left) and urea (Figure 4G, right). Next, the hESC-derived HBCs were differentiated into cholangiocyte-like cells as described in Figure 4H. After 2 weeks of biliary differentiation, tubular structures (Figure 4I) that were CK7 positive (Figure 4J) were observed. Although the gene expression levels of mature hepatocyte markers (Figure 4K) in the HBC P0-, HBC P10-, or HBC clone-derived cholangiocyte-like cells did not change, the gene expression levels of mature cholangiocyte markers (Figure 4L) in these cells were higher than those in the cells that had not undergone differentiation. Similar results were obtained by using another hESC line (H1) and hiPSC line (Dotcom) (Figure S4). Moreover, HBC-derived hepatocyte-like cells exhibited CYP metabolism capacity (Figure S5A) and a functional urea cycle that could response to ammonia (Figure S5B) and were considered to have potential to be applied in the prediction of drug-induced hepatotoxicity (Figure S5C). Taken together, these results indicated that the hPSC-derived HBCs have the ability to differentiate into both hepatic and biliary lineages in vitro.

In Vivo Cell Transplantation Assays of the hPSC-Derived HBCs

To examine whether the hESC-derived HBCs could be used for hepatocyte transplantation, these cells were transplanted into CCl_4-treated immunodeficient mice as shown in Figure 5A. The hepatocyte functionality of the hESC-derived HBC P0 or HBC P10 was assessed by measuring secreted human ALB levels in the recipient mice (Figure 5B). Although human ALB was detected in the mice that were transplanted with the hESC-derived HBC P0 or HBC P10, it was not detected in the mice that were not transplanted with these cells. The ALB-positive cells were observed in mice transplanted with the hESC-derived HBC P0 or HBC P10 (Figure 5C). Most of the ALB-positive cells in mice transplanted with the hESC-derived HBC P10 were AFP negative (Figure 5D), indicating that transplanted hESC-derived HBCs were differentiated into mature hepatocyte-like cells (some of them were binuclear [Figure 5E, white arrows]). These results demonstrated that hESC-derived HBCs have the potential to be applied for hepatocyte transplantation.

(C) The hESC-derived cells (day 9) were plated onto a human LN111, 211, 411, or 511-coated dish. The percentage of AFP-positive cells was examined by using FACS analysis on day 9 (before passage and after passage [HBC P0]) or day 16. Data represent the mean ± SD from three independent experiments.
(D) The hESC-derived cells cultured on a human LN111-coated dish for 7 days were subjected to immunostaining with anti-AFP (green) antibodies.
(E) The hESC-derived cells (day 9) were plated onto human LN111, 211, 411, or 511-coated dishes. The gene expression levels of *AFP* and pan-hepatoblast markers (*CD133*, *EpCAM*, *CK8*, and, *CK18*) were measured by real-time RT-PCR on day 16. The gene expression levels in the hESC-derived HBCs (the LN111-attached cells were collected at 15 min after plating) were taken as 1.0.
(F) The HBCs derived from hESCs (H9) or hiPSCs (Dotcom) were cultured and cell growth was analyzed by obtaining a cell count at each passage. Data represent the mean ± SD from three independent experiments.
(G) The percentage of AFP-positive cells was examined by using FACS analysis on day 9 (before passage), P1 (HBCs passaged once), P10 (HBCs passaged ten times), and P15 (HBCs passaged 15 times). Data represent the mean ± SD from seven independent experiments.
See also Tables S2 and S3.

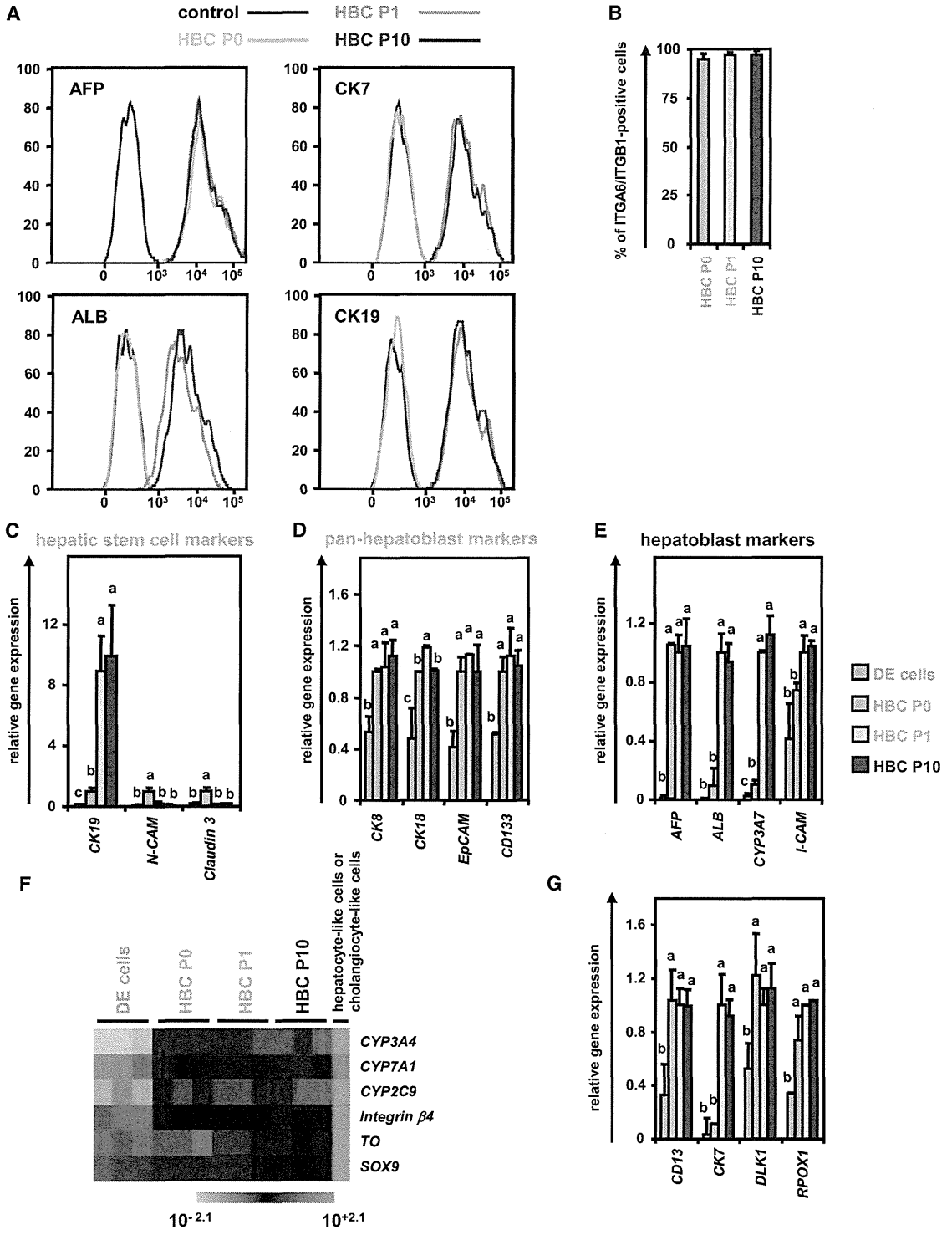

Figure 3. The hESC-Derived HBCs Were Characterized

(A and B) The hESCs (H9) were differentiated according to Figure 1A and then passaged onto a human LN111-coated dish. The attached cells (hESC-derived HBCs [HBC P0]) were collected at 15 min after plating. The percentage of AFP-positive, ALB-positive, CK7-positive, CK19-positive (A), and integrin α6- and integrin β1-double positive (B) cells in the hESC-derived HBC P0, HBC P1 (HBCs passaged once), and HBC P10 (HBCs passaged ten times) populations was estimated by using FACS analysis. Data represent the mean ± SD from seven independent experiments.

(legend continued on next page)

DISCUSSION

The main purpose of this study was to establish and characterize expandable HBCs from hPSCs. First, we identified that human LN111 could support self-renewal and proliferation of hPSC-derived HBCs in the presence of HGF and EGF. Second, we showed that the hPSC-derived HBCs have the potential to segregate into both hepatic and biliary lineages, and to integrate into the mouse liver parenchyma.

We have demonstrated that the hPSC-derived HBCs could be maintained on a human LN111-coated dish in an integrin α6- and β1-dependent manner (Figure 1). It is known that undifferentiated hPSCs could be maintained on a human LN511-coated dish but not on a human LN111-coated dish (Rodin et al., 2010). This might suggest that human LN111 has the potential not only to selectively maintain HBCs, but also to eliminate residual undifferentiated cells. Our hepatoblast-like cells could efficiently proliferate for more than 3 months on a human LN111-coated dish (Figure 2). In the human liver development (during 5–10 weeks gestation), laminin is observed in both the perisinusoidal space and portal tracts (Couvelard et al., 1998). The expression of laminin is localized around the periportal biliary trees during the later stage of liver development (Couvelard et al., 1998). Hepatic stem cells reside around the hepatic portal area (Clément et al., 1988). It is also known that laminin is accumulated around oval cells although laminin is not expressed around quiescent mature hepatocytes (Paku et al., 2001). These facts suggest that laminin plays an important role in the maintenance and proliferation of hepatoblasts.

The hPSC-derived HBC P10 and clone were positive for hepatoblast markers (AFP, ALB, CYP3A7, and I-CAM), but negative for hepatic stem cell markers (N-CAM and Claudin 3) (Figure 3) (Schmelzer et al., 2007). Although the hPSC-derived HBCs were able to expand on human LN111-coated dish, Schmelzer et al. showed that human hepatoblasts do not proliferate under a monolayer culture condition, but human hepatic stem cells could self-replicate for more than 6 months (Schmelzer et al., 2007). Although further investigations of the hepatoblast characteristics in the hPSC-derived HBCs will be needed in the future, the results in the present study suggest that the characteristics of hPSC-derived HBCs expanded on human LN111-coated dishes were similar to those in human hepatoblasts isolated from the human liver (Schmelzer et al., 2007; Zhang et al., 2008).

The hPSC-derived HBCs had the ability to integrate into the mouse liver parenchyma (Figure 5), in the manner of human hepatic stem cells or hepatoblasts (Schmelzer et al., 2007). The human ALB serum levels (approximately 20–70 ng/ml) in mice transplanted with the hESC-derived HBC P0 or HBC P10 were comparable to those in the previous paper in which the hESC-derived definitive endoderm cells, hepatoblasts, and hepatocyte-like cells were transplanted into mice (Liu et al., 2011), but were lower than those of human liver chimeric mice (Tateno et al., 2004). Human ALB serum levels would increase if more suitable host mice, such as urokinase plasminogen activator-SCID mice were used (Tateno et al., 2004).

In this study, we have developed a technology for the maintenance and proliferation of hPSC-derived HBCs by using human LN111. To transplant these cells for purposes of regenerative medicine, a xeno-free culture condition for hPSC-derived HBCs must be developed in the future. It is hoped that the hPSC-derived HBCs and their derivatives will be helpful in various medical applications, such as drug screening and regenerative medicine.

EXPERIMENTAL PROCEDURES

hESC and hiPSC Culture

The hESC lines (H1 [WA01] and H9 [WA09] [WiCell Research Institute]) and the hiPSC line, Dotcom (JCRB number: JCRB1327) (Makino et al., 2009; Nagata et al., 2009), were maintained on a feeder layer of mitomycin-C-treated mouse embryonic fibroblasts (Millipore) with ReproStem medium (ReproCELL) supplemented with 5 and 10 ng/ml fibroblast growth factor 2 (FGF2) (Katayama Kagaku Kogyo), respectively. H1 and H9 were used following the Guidelines for Derivation and Utilization of Human Embryonic Stem Cells of the Ministry of Education, Culture, Sports, Science and Technology of Japan, and, furthermore, the study was approved by an independent ethics committee.

In Vitro Hepatoblast Differentiation

The differentiation protocol for the induction of definitive endoderm cells and hepatoblasts was based on our previous report with some modifications (Inamura et al., 2011; Takayama et al., 2012a, 2012b, 2013). In mesendoderm differentiation, hESCs/iPSCs were

(C–F) The gene expression levels of hepatic stem cell markers (C), pan-hepatoblast markers (D), hepatoblast markers (E), and mature hepatocyte (*CYP3A4*, *7A1*, *2C9*, and *TO*) or cholangiocyte markers (*integrin β4* and *SOX9*) (F) were measured in the definitive endoderm cells, HBC P0, HBC P1, or HBC P10 by real-time RT-PCR.

(G) The gene expression levels of *CD13*, *CK7*, *DLK1*, and *PROX1* were measured in the hESC-derived definitive endoderm cells, HBC P0, HBC P1, or HBC P10 by real-time RT-PCR. Data represent the mean ± SD from three independent experiments. Statistical significance was evaluated by ANOVA followed by Bonferroni post hoc tests to compare four groups (DE cells, HBC P0, HBC P1, and HBC P10). Groups that do not share the same letter are significantly different from each other ($p < 0.05$). DE, definitive endoderm cells.

See also Figures S2 and S3 and Tables S2–S4.

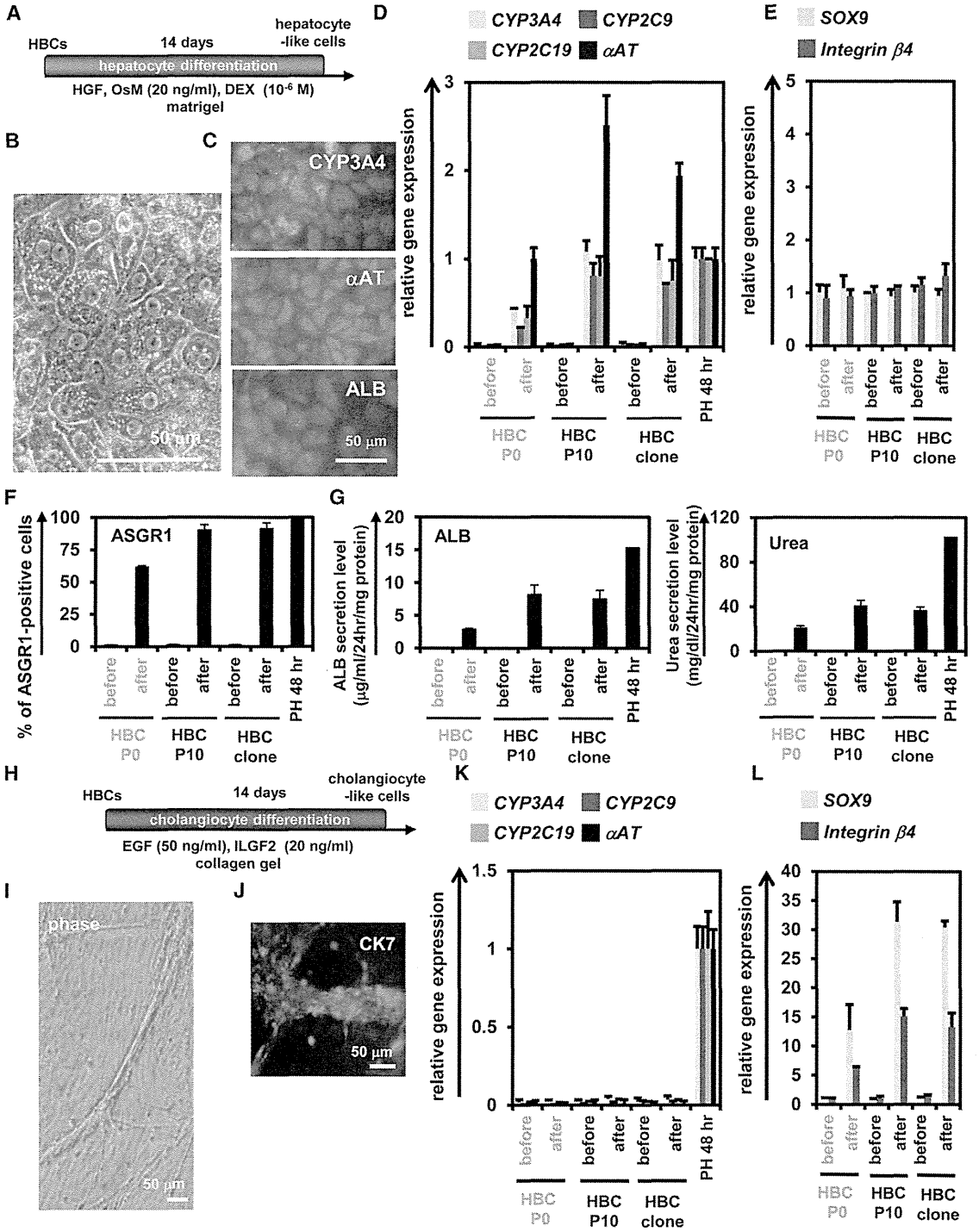

Figure 4. The hESC-Derived HBCs Could Differentiate into Both Hepatic and Biliary Lineages

(A) The procedure for differentiation of the hESC (H9)-derived HBC P0, HBC P10, or HBC clone into the hepatocyte-like cells is presented schematically. Details are described in Experimental Procedures.

(B) Phase-contrast micrographs of the HBC P10-derived hepatocyte-like cells are shown.

(C) The HBC P10-derived hepatocyte-like cells were subjected to immunostaining with anti-CYP3A4 (green), anti-αAT (red), and anti-ALB (red) antibodies.

(D and E) The gene expression levels of hepatocyte (D) or cholangiocyte (E) markers in HBC P0-, HBC P10-, or HBC clone-derived hepatocyte-like cells were measured by real-time RT-PCR after 14 days of hepatocyte differentiation. In (D), the gene expression levels in

(legend continued on next page)

cultured for 2 days on Matrigel (BD Biosciences) in differentiation hESF-DIF medium that contains 100 ng/ml Activin A (R&D Systems) (hESF-DIF medium was purchased from Cell Science & Technology Institute; differentiation hESF-DIF medium was supplemented with 10 μg/ml human recombinant insulin, 5 μg/ml human apotransferrin, 10 μM 2-mercaptoethanol, 10 μM ethanolamine, 10 μM sodium selenite, and 0.5 mg/ml bovine fatty acid free serum albumin [all from Sigma]). To generate definitive endoderm cells, the mesendoderm cells (day 2) were transduced with 3,000 vector particle (VP)/cell of FOXA2-expressing adenovirus vectors (Ad-FOXA2) for 1.5 hr and cultured until day 6 on Matrigel in differentiation hESF-DIF medium supplemented with 100 ng/ml Activin A. For induction of hepatoblasts, the definitive endoderm cells were cultured for 3 days on a Matrigel in differentiation hESF-DIF medium supplemented with 30 ng/ml bone morphogenetic protein 4 (BMP4) (R&D Systems) and 20 ng/ml FGF4 (R&D Systems).

Establishment and Maintenance of the hPSC-Derived HBCs

The hPSC-derived HBCs were first purified from the hPSC-derived cells (day 9) by selecting attached cells on a human recombinant LN111 (BioLamina)-coated dish at 15 min after plating. The hPSC-derived HBCs were cultured on a human LN111-coated dish (2.0×10^4 cells/cm^2) in maintenance DMEM/F12 medium (DMEM/F12 medium [Invitrogen] was supplemented with 10% FBS, 1 × insulin/transferrin/selenium, 10 mM nicotinamide, 10^{-7} M dexamethasone (DEX) (Sigma), 20 mM HEPES, 25 mM $NaHCO_3$, 2 mM L-glutamine, penicillin/streptomycin, 40 ng/ml hepatocyte growth factor [HGF] [R&D Systems] and 20 ng/ml epidermal growth factors [EGF] [R&D Systems]). The medium was refreshed every day. The hPSC-derived HBCs were dissociated with Accutase (Millipore) into single cells and subcultured every 6 or 7 days.

Establishment and Maintenance of a Single hPSC-Derived HBC

For single-cell culture, the single HBC was plated to separate well of human LN111-coated 96-well plate in maintenance DMEM/F12 medium supplemented with 25 μM Y-27632 (ROCK inhibitor) (Millipore), and then colonies derived from a single cell were manually picked up and cultured as well as HBCs (these cells were designated the HBC clone).

In Vitro Hepatocyte and Cholangiocyte Differentiation

To induce hepatocyte differentiation, the hPSC-derived HBC P0, HBC P10, and HBC clone were cultured for 14 days on a Matrigel-coated dish (7.5×10^4 cells/cm^2) in HCM (Lonza) supplemented with 20 ng/ml HGF, 20 ng/ml Oncostatin M (OsM) (R&D Systems), and 10^{-6} M DEX. To induce cholangiocyte differentiation, the hPSC-derived HBC P0, HBC P10, and HBC clone were cultured in collagen gel for 14 days. To establish collagen gel plates, 500 μl collagen gel solution (consisting of 400 μl type I-A Collagen (Nitta gelatin), 50 μl 10 × DMEM, and 50 μl of 200 mM HEPES buffer containing 2.2% $NaHCO_3$ and 0.05 M NaOH) was added to each well, and then the plates were incubated at 37°C for 30 min. The hPSC-derived HBC P0, HBC P10, and HBC clone (5×10^4 cells) were resuspended in 500 μl differentiation DMEM/F12 medium (differentiation DMEM/F12 medium was supplemented with 20 mM HEPES, 2 mM L-glutamine, 100 ng/ml EGF, and 40 ng/ml insulin-like growth factor 2 [ILGF2]), and then mixed with 500 μl of the collagen gel solution and plated onto the basal layer of collagen. After 30 min, 2 ml of differentiation DMEM/F12 medium was added to the well.

Ad Vectors

Ad vectors were constructed by an improved in vitro ligation method. The human EF-1α promoter-driven FOXA2-expressing Ad vectors (Ad-FOXA2) were constructed previously (Takayama et al., 2012b). All of Ad vectors contain a stretch of lysine residue (K7) peptides in the C-terminal region of the fiber knob for more efficient transduction of hESCs, hiPSCs, mesendoderm cells, and definitive endoderm cells, in which transfection efficiency was almost 100%, and purified as described previously (Inamura

PH 48 hr were taken as 1.0. In (E), the gene expression levels in HBC P10 (before differentiation) were taken as 1.0. Data represent the mean ± SD from three independent experiments. Student's t test indicated that gene expression levels of the hepatocyte markers in "after" were significantly higher than those in "before" ($p < 0.01$).
(F) The efficiency of hepatocyte differentiation was measured by estimating the percentage of ASGR1-positive cells using FACS analysis.
(G) The amounts of ALB (left) and urea (right) secretion were examined. Data represent the mean ± SD from three independent experiments. Student's t test indicated that the percentage of ASGR1-positive cells, the ALB secretion level, and urea secretion level in "after" were significantly higher than those in "before" ($p < 0.01$).
(H) The procedure for the differentiation of the hESC-derived HBC P0, HBC P10, or HBC clone into cholangiocyte-like cells is presented schematically. Details are described in Experimental Procedures.
(I) Phase-contrast micrographs of the HBC P10-derived cholangiocyte-like cells are shown.
(J) The HBC P10-derived cholangiocyte-like cells were subjected to immunostaining with anti-CK7 (red) antibodies.
(K and L) The gene expression levels of hepatocyte (K) or cholangiocyte (L) markers in the HBC P0-, HBC P10-, or HBC clone-derived cholangiocyte-like cells were measured by real-time RT-PCR after 14 days of cholangiocyte differentiation. In (K), the gene expression levels in PH 48 hr were taken as 1.0. In (L), the gene expression levels in HBC P10 (before cholangiocyte differentiation) were taken as 1.0. Data represent the mean ± SD from three independent experiments. Student's t test indicated that the gene expression levels of cholangiocyte markers in "after" were significantly higher than those in "before" ($p < 0.01$). "Before" indicates the HBCs before hepatocyte or cholangiocyte differentiation; "After" indicates the HBCs after hepatocyte or cholangiocyte differentiation.
See also Figures S4 and S5 and Tables S1–S4.

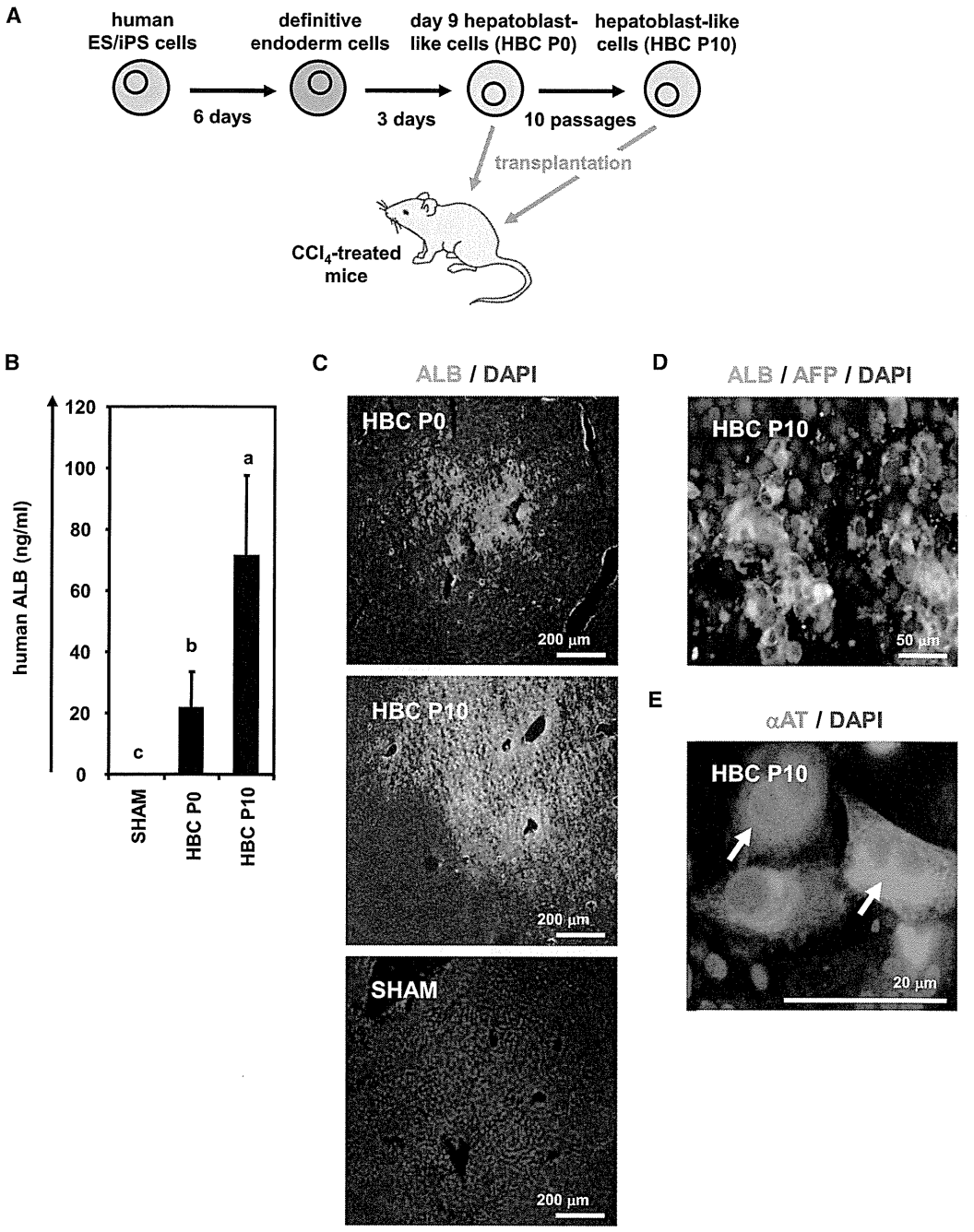

Figure 5. The hESC-Derived HBCs Were Integrated into the Mouse Liver Parenchyma

(A) The procedure for transplantation of the hESC (H9)-derived HBC P0 and HBC P10 into CCl_4 (4 ml/kg)-treated Rag2/IL2 receptor gamma double-knockout mice is presented schematically.

(B) The human ALB level in recipient mouse serum was measured at 2 weeks after transplantation. Data represent the mean ± SD from six to eight mice in each group. Statistical significance was evaluated by ANOVA followed by Bonferroni post hoc tests to compare all groups. Groups that do not share the same letter are significantly different from each other ($p < 0.05$).

(C) Expressions of the ALB (green) in the liver of transplanted mice were examined by immunohistochemistry at 2 weeks after transplantation.

(D and E) The expressions of AFP (red), ALB (green) (D), and αAT (red) (E) were examined by immunohistochemistry at 2 weeks after hESC-derived HBC P10 transplantation. White arrows show transplanted cells, which have double nuclei.

See also Tables S2 and S3.

et al., 2011; Takayama et al., 2011; Tashiro et al., 2010). The VP titer was determined by using a spectrophotometric method.

Flow Cytometry

Single-cell suspensions of the hPSC-derived cells were fixed with 4% paraformaldehyde (PFA) at 4°C for 10 min and then incubated with the primary antibody (described in Table S2), followed by the secondary antibody (described in Table S3). Control cells were incubated with anti-mouse, goat, or rabbit immunoglobulin (Ig) G antibodies (Santa Cruz Biotechnology) and then incubated with the secondary antibody. Flow cytometry analysis was performed using a fluorescence-activated cell sorting (FACS) LSR Fortessa flow cytometer (BD Biosciences). Cell sorting was performed using a FACS Aria (BD Biosciences).

RNA Isolation and RT-PCR

Total RNA was isolated from hPSCs and their derivatives using ISOGENE (Nippon Gene). cDNA was synthesized using 500 ng of total RNA with a Superscript VILO cDNA synthesis kit (Invitrogen). Real-time RT-PCR was performed with SYBR green PCR Master Mix (Applied Biosystems) using an Applied Biosystems StemOnePlus real-time PCR systems. Relative quantification was performed against a standard curve, and the values were normalized against the input determined for the housekeeping gene, glyceraldehyde 3-phosphate dehydrogenase. The primer sequences used in this study are described in Table S4. In addition, we confirmed that every beta integrin primer used in this manuscript showed a similar amplification efficacy (Table S5). The amplification efficiency was calculated from the slope of the standard curve according to the following formula: e = 10^(−1/slope)-1. Every beta integrin primer used in this manuscript showed a similar amplification efficacy.

Immunohistochemistry

The cells were fixed with 4% PFA for 15 min and then blocked with PBS containing 2% FBS, 2% bovine serum albumin (BSA), and 0.1% Triton X-100 (Wako Pure Chemicals Industries) for 1 hr. The cells were incubated with primary antibody (described in Table S2) at 4°C for overnight, followed by incubation with a secondary antibody (described in Table S3) at room temperature for 1 hr. Nuclei were counterstained with DAPI (blue).

ELISA

The hPSC-derived HBC P0, HBC P10, and HBC clone were differentiated into the hepatocyte-like cells as described in Figure 4A. The culture supernatants, which were incubated for 24 hr after fresh medium was added, were collected and analyzed for the amount of ALB secretion by ELISA. ELISA kits for ALB were purchased from Bethyl Laboratories. The amount of ALB secretion was calculated according to each standard followed by normalization to the protein content per well. The human ALB amount in mice serum was also examined by ELISA.

Transplantation of the hESC-Derived HBCs

The hESC-derived HBCs were dissociated using accutase and then suspended with maintenance DMEM/F12 medium without serum. Eight- to 10-week-old Rag2/IL2Rg double-knockout mice were prepared. The hESC-derived HBCs (1×10^6 cells) were transplanted 24 hr after administration of CCl_4 (4 ml/kg) by intrasplenical injection. Recipient mouse liver and blood were harvested at 2 weeks after transplantation. The livers were fixed with 4% PFA and processed for immunohistochemistry. Human hepatocytes producing the ALB, AFP, and αAT protein were identified in mouse liver by an antibody specifically recognizing human but not mouse albumin. In addition, serum was extracted and subjected to ELISA analysis. All animal experiments were conducted in accordance with institutional guidelines.

Urea Secretion

The hPSC-derived HBC P0, HBC P10, and HBC clone were differentiated into hepatocyte-like cells as described in Figure 4A. The culture supernatants, which were incubated for 24 hr after fresh medium was added, were collected and analyzed for the amount of urea secretion. The urea measurement kits were purchased from BioAssay Systems. The amount of urea secretion was calculated according to each standard followed by normalization to the protein content per well. In Figure S5B, both the HBC-derived hepatocyte-like cells and primary human hepatocytes (PHs) (three lots of cryopreserved human hepatocytes were used), that were cultured for 48 hr after the cells were plated (PH 48 hr), were cultured in HCM (containing glutamine) or DMEM (not containing glutamine; Wako) in the presence or absence of 1 mM ammonium chloride (NH_4Cl, Wako) for 24 hr, and then the amount of urea secretion was measured.

Primary Human Hepatocytes

Three lots of cryopreserved human hepatocytes (lot Hu8072 [CellzDirect], HC2-14, and HC10-101 [Xenotech]) were used. The vials of hepatocytes were rapidly thawed in a shaking water bath at 37°C; the contents of the vial were emptied into prewarmed Cryopreserved Hepatocyte Recovery Medium (Gibco) and the suspension was centrifuged at 100 g for 10 min at room temperature. The hepatocytes were seeded at 1.25×10^5 cells/cm^2 in HCM (Lonza) containing 10% fetal calf serum (FCS) (Gibco) onto type I collagen-coated 12-well plates. The medium was replaced with hepatocyte culture medium containing 10% FCS 6 hr after seeding. The hepatocytes, which were cultured 48 hr after plating the cells, were used in the experiments.

Adhesion-Blocking Assay Using Integrin Antibody

Twelve-well plates were coated with human recombinant LN111, 211, 411, or 511 (all from BioLamina) and blocked by 1% heat-denatured BSA containing PBS. The hESC-derived single cells were incubated with function-blocking antibodies to integrin α6 and β1 (at the concentrations as recommended by the manufacturer) for 30 min, plated on a human LN111-coated 12-well dish, and allowed to adhere for 1 hr at 37°C. After unattached cells were removed, the remaining adherent cells were fixed for 20 min with 5% glutaraldehyde. The hESC-derived cells that had adhered to the wells were stained with 200 μl of 0.3% crystal violet (Wako) solution at room temperature for 15 min. Excess crystal violet was then removed, and the wells were washed three times. Fixed crystal violet was solubilized in 200 μl of 100% ethanol at room

temperature for 15 min. Cell viability was estimated by measuring the absorbance at 595 nm of each well using a microtiter plate reader (Sunrise, Tecan).

CYP Activity

To measure the CYP1A2, 2C9, and 3A4 activity of the cells, we performed lytic assays by using P450-GloTM CYP1A2, 2C9, and 3A4 Assay Kits (Promega), respectively. We measured the fluorescence activity with a luminometer (Lumat LB 9507; Berthold) according to the manufacturer's instructions. The CYP activity was normalized with the protein content per well.

Karyotyping

This experiment was carried out at Chromosome Science Labo.

Cell Viability Tests

Cell viability was assessed by using a WST-8 assay kit (Dojindo), and the results are presented in Figure S5C. After treatment with test compounds, such as acetaminophen (Wako) and troglitazone (Wako) for 24 hr, the cell viability was measured. The control cells were incubated in the absence of test compounds and were considered to have 100% viability value. Controls were treated with DMSO (final concentration 0.1%).

SUPPLEMENTAL INFORMATION

Supplemental Information includes five figures and five tables and can be found with this article online at http://dx.doi.org/10.1016/j.stemcr.2013.08.006.

ACKNOWLEDGMENTS

We thank Yasuko Hagihara for her excellent technical support. H.M., K.K., and T.H. were supported by grants from the Ministry of Health, Labor, and Welfare of Japan. H.M. was also supported by the Project for Technological Development of the Japan Science and Technology Agency (JST) and by the Uehara Memorial Foundation. F.S. was supported by Program for Promotion of Fundamental Studies in Health Sciences of the National Institute of Biomedical Innovation. K.T. and Y.N. are Research Fellows of the Japan Society for the Promotion of Science.

Received: June 6, 2013
Revised: August 27, 2013
Accepted: August 27, 2013
Published: October 3, 2013

REFERENCES

Clément, B., Rescan, P.Y., Baffet, G., Loréal, O., Lehry, D., Campion, J.P., and Guillouzo, A. (1988). Hepatocytes may produce laminin in fibrotic liver and in primary culture. Hepatology *8*, 794–803.

Couvelard, A., Bringuier, A.F., Dauge, M.C., Nejjari, M., Darai, E., Benifla, J.L., Feldmann, G., Henin, D., and Scoazec, J.Y. (1998). Expression of integrins during liver organogenesis in humans. Hepatology *27*, 839–847.

Hay, D.C., Zhao, D., Fletcher, J., Hewitt, Z.A., McLean, D., Urruticoechea-Uriguen, A., Black, J.R., Elcombe, C., Ross, J.A., Wolf, R., and Cui, W. (2008). Efficient differentiation of hepatocytes from human embryonic stem cells exhibiting markers recapitulating liver development in vivo. Stem Cells *26*, 894–902.

Inamura, M., Kawabata, K., Takayama, K., Tashiro, K., Sakurai, F., Katayama, K., Toyoda, M., Akutsu, H., Miyagawa, Y., Okita, H., et al. (2011). Efficient generation of hepatoblasts from human ES cells and iPS cells by transient overexpression of homeobox gene HEX. Mol. Ther. *19*, 400–407.

Kamiya, A., Kakinuma, S., Yamazaki, Y., and Nakauchi, H. (2009). Enrichment and clonal culture of progenitor cells during mouse postnatal liver development in mice. Gastroenterology *137*, 1114–1126.

Liu, H., Kim, Y., Sharkis, S., Marchionni, L., and Jang, Y.Y. (2011). In vivo liver regeneration potential of human induced pluripotent stem cells from diverse origins. Sci. Transl. Med. *3*, 82ra39.

Makino, H., Toyoda, M., Matsumoto, K., Saito, H., Nishino, K., Fukawatase, Y., Machida, M., Akutsu, H., Uyama, T., Miyagawa, Y., et al. (2009). Mesenchymal to embryonic incomplete transition of human cells by chimeric OCT4/3 (POU5F1) with physiological co-activator EWS. Exp. Cell Res. *315*, 2727–2740.

Nagata, S., Toyoda, M., Yamaguchi, S., Hirano, K., Makino, H., Nishino, K., Miyagawa, Y., Okita, H., Kiyokawa, N., Nakagawa, M., et al. (2009). Efficient reprogramming of human and mouse primary extra-embryonic cells to pluripotent stem cells. Genes Cells *14*, 1395–1404.

Paku, S., Schnur, J., Nagy, P., and Thorgeirsson, S.S. (2001). Origin and structural evolution of the early proliferating oval cells in rat liver. Am. J. Pathol. *158*, 1313–1323.

Rodin, S., Domogatskaya, A., Ström, S., Hansson, E.M., Chien, K.R., Inzunza, J., Hovatta, O., and Tryggvason, K. (2010). Long-term self-renewal of human pluripotent stem cells on human recombinant laminin-511. Nat. Biotechnol. *28*, 611–615.

Schmelzer, E., Zhang, L., Bruce, A., Wauthier, E., Ludlow, J., Yao, H.L., Moss, N., Melhem, A., McClelland, R., Turner, W., et al. (2007). Human hepatic stem cells from fetal and postnatal donors. J. Exp. Med. *204*, 1973–1987.

Sumi, T., Tsuneyoshi, N., Nakatsuji, N., and Suemori, H. (2008). Defining early lineage specification of human embryonic stem cells by the orchestrated balance of canonical Wnt/beta-catenin, Activin/Nodal and BMP signaling. Development *135*, 2969–2979.

Takayama, K., Inamura, M., Kawabata, K., Tashiro, K., Katayama, K., Sakurai, F., Hayakawa, T., Furue, M.K., and Mizuguchi, H. (2011). Efficient and directive generation of two distinct endoderm lineages from human ESCs and iPSCs by differentiation stage-specific SOX17 transduction. PLoS ONE *6*, e21780.

Takayama, K., Inamura, M., Kawabata, K., Katayama, K., Higuchi, M., Tashiro, K., Nonaka, A., Sakurai, F., Hayakawa, T., Furue, M.K., and Mizuguchi, H. (2012a). Efficient generation of functional hepatocytes from human embryonic stem cells and induced pluripotent stem cells by HNF4α transduction. Mol. Ther. *20*, 127–137.

Takayama, K., Inamura, M., Kawabata, K., Sugawara, M., Kikuchi, K., Higuchi, M., Nagamoto, Y., Watanabe, H., Tashiro, K., Sakurai,

F., et al. (2012b). Generation of metabolically functioning hepatocytes from human pluripotent stem cells by FOXA2 and HNF1α transduction. J. Hepatol. *57*, 628–636.

Takayama, K., Kawabata, K., Nagamoto, Y., Kishimoto, K., Tashiro, K., Sakurai, F., Tachibana, M., Kanda, K., Hayakawa, T., Furue, M.K., and Mizuguchi, H. (2013). 3D spheroid culture of hESC/hiPSC-derived hepatocyte-like cells for drug toxicity testing. Biomaterials *34*, 1781–1789.

Tanimizu, N., Saito, H., Mostov, K., and Miyajima, A. (2004). Long-term culture of hepatic progenitors derived from mouse Dlk+ hepatoblasts. J. Cell Sci. *117*, 6425–6434.

Tashiro, K., Kawabata, K., Inamura, M., Takayama, K., Furukawa, N., Sakurai, F., Katayama, K., Hayakawa, T., Furue, M.K., and Mizuguchi, H. (2010). Adenovirus vector-mediated efficient transduction into human embryonic and induced pluripotent stem cells. Cell Reprogram. *12*, 501–507.

Tateno, C., Yoshizane, Y., Saito, N., Kataoka, M., Utoh, R., Yamasaki, C., Tachibana, A., Soeno, Y., Asahina, K., Hino, H., et al. (2004). Near completely humanized liver in mice shows human-type metabolic responses to drugs. Am. J. Pathol. *165*, 901–912.

Zhang, L., Theise, N., Chua, M., and Reid, L.M. (2008). The stem cell niche of human livers: symmetry between development and regeneration. Hepatology *48*, 1598–1607.

Zhao, D., Chen, S., Cai, J., Guo, Y., Song, Z., Che, J., Liu, C., Wu, C., Ding, M., and Deng, H. (2009). Derivation and characterization of hepatic progenitor cells from human embryonic stem cells. PLoS ONE *4*, e6468.

FEBS Open Bio 3 (2013) 387–393

ELSEVIER

CrossMark

FEBS openbio

journal homepage: www.elsevier.com/locate/febsopenbio

Identification, expression and characterization of rat isoforms of the serum response factor (SRF) coactivator MKL1☆

Mitsuru Ishikawa[a,1], Jun Shiota[a,1], Yuta Ishibashi[a,1], Tomoyuki Hakamata[a,1], Shizuku Shoji[a], Mamoru Fukuchi[a], Masaaki Tsuda[a], Tomoaki Shirao[b], Yuko Sekino[c], Toshihisa Ohtsuka[d], Jay M. Baraban[e], Akiko Tabuchi[a,*]

[a] Laboratory of Molecular Neurobiology, Graduate School of Medicine and Pharmaceutical Sciences, University of Toyama, 2630 Sugitani, Toyama 930-0194, Japan
[b] Department of Neurobiology and Behavior, Gunma University, Graduate School of Medicine, 3-39-22 Showa-machi, Maebashi 371-8511, Japan
[c] Division of Pharmacology, Biological Safety Research Center, National Institute of Health Sciences, 1-18-1 Kamiyoga, Setagaya-ku, Tokyo 158-8501, Japan
[d] Department of Biochemistry, Graduate School of Medicine/Faculty of Medicine, University of Yamanashi, 1110 Shimokato, Chuo, Yamanashi 409-3898, Japan
[e] Solomon H. Snyder Department of Neuroscience, Johns Hopkins University, School of Medicine, 725 North Wolfe Street, Baltimore, MD 21205, USA

ARTICLE INFO

Article history:
Received 5 June 2013
Received in revised form 21 August 2013
Accepted 4 September 2013

Keywords:
Megakaryoblastic leukemia
Serum response factor
Transcript
Alternative promoter
Transcriptional coactivator

ABSTRACT

Megakaryoblastic leukemia 1 (MKL1) is a member of the MKL family of serum response factor (SRF) coactivators. Here we have identified three rat MKL1 transcripts: two are homologues of mouse MKL1 transcripts, full-length MKL1 (FLMKL1) and basic, SAP, and coiled-coil domains (BSAC), the third is a novel transcript, MKL1-elongated derivative of yield (MELODY). These rat MKL1 transcripts are differentially expressed in a wide variety of tissues with highest levels in testis and brain. During brain development, these transcripts display differential patterns of expression. The FLMKL1 transcript encodes two isoforms that utilize distinct translation start sites. The longer form possesses three actin-binding RPXXXEL (RPEL) motifs and the shorter form, MKL1met only has two RPEL motifs. All four rat MKL1 isoforms, FLMKL1, BSAC, MKL1met and MELODY increased SRF-mediated transcription, but not CREB-mediated transcription. Accordingly, the differential expression of MKL1 isoforms may help fine-tune gene expression during brain development.

1. Introduction

The megakaryoblastic leukemia (MKL) family members, MKL1 and MKL2, function as serum response factor (SRF) coactivators [1–5]. Several studies conducted in non-neuronal cells have shown that MKL1 binds to G-actin via its RPXXXEL (RPEL) motifs and translocates into the nucleus where it binds to and activates SRF in response to actin polymerization and G-actin depletion [6–8]. MKL1 and MKL2 regulate a set of genes that code for cytoskeletal proteins and are involved in alteration of cell shape and motility [5]. MKL family members are also highly expressed in the brain and they regulate morphology of cultured cortical or hippocampal neurons [9–12].

MKL1 isoforms were initially identified in non-neuronal cells. One of the mouse MKL1 cDNAs derived from NIH3T3 cells has two alternative translation start sites; the upstream site uses leucine as the initiator codon and generates full-length MAL/MKL1, MAL/MKL1(fl), while the downstream site employs methionine as the start codon to produce a shorter protein, MAL/MKL1(met) [6]. Another MAL/MKL1 transcript, called BSAC (basic, SAP and coiled-coil domain) has been identified in mouse spleen which contains a 5′-exon different from that of the MAL/MKL1(fl) transcript [2]. Mouse MAL/MKL1 (fl) and MAL/MKL1met are able to translocate from the cytoplasm to the nucleus in response to serum-stimulation in NIH3T3 cells [6]. As MKL1 is expressed prominently in brain and plays a key role in regulating neuronal morphology, we sought to define the pattern of expression of MKL1 transcripts during brain development and whether MKL1 isoforms differ in their ability to regulate SRF-mediated transcription. In the course of these studies, we have identified a novel MKL1 transcript termed MKL1-elongated derivative of yield (MELODY) and two MKL1 transcripts which have homology to mouse MAL/MKL1(fl) and BSAC. Furthermore, we have found that: (1) these MKL1 isoforms are differentially expressed during brain development, and (2) MELODY, in addition to FLMKL1, BSAC and MKL1met, activates SRF-mediated

Abbreviations: BSAC, basic, SAP, and coiled-coil domains; DAPI, 4′, 6-diamidino-2-phenylindole; GFP, green fluorescent protein; MAL, megakaryocytic acute leukemia; MKL1, megakaryoblastic leukemia 1; MELODY, MKL1-elongated derivative of yield; RPEL, arginine proline XXX glutamate leucine; SRF, serum response factor.

[1] These authors equally contributed to this work.

* Corresponding author. Tel.: +81 76 434 7536; fax: +81 76 434 5048.
E-mail address: atabuchi@pha.u-toyama.ac.jp (A. Tabuchi).

2211-5463/$36.00
http://dx.doi.org/10.1016/j.fob.2013.09.001

transcription.

2. Materials and methods

2.1. Animals

Male SD rats for measuring MKL1 mRNA expression were purchased from Sankyo Labo Service Corporation, Inc. (Tokyo, Japan). All experiments were carried out in accordance with the guidelines of the Animal Care and Experimentation Committee of University of Toyama, Sugitani Campus. The protocols were approved as permit numbers (S-2008 PHA-3, S2009 PHA-23, S2010 PHA-1, A2011 PHA-5, A2012 PHA-1). Every effort was made to minimize suffering.

2.2. Cloning of rat MKL1 transcripts

To clone cDNA of rat MKL1 transcripts, the following primers for 5′-rapid amplification cDNA-end (5′-RACE) were initially designed based on the predicted rat MKL1 mRNA sequence (NCBI Reference Sequence: XM_235497.4), which was derived by sequence tagged sites (STS) and expressed sequence tags (EST). The primers correspond to the predicted exons 7 and 8: RT (5′-TCTCATTGAGGTC-3′), sense1 (5′-GAGCCTTCTCTCCAGGCCAA-3′), antisense1 (5′-AGGTCTCTTCCAGAATGTGC-3′), sense2 (5′-GCTGAAGCTGAAGAGAGCCA-3′), antisense2 (5′-CCTGACCAGCTCTGATCTCT-3′). The 5′-RACE procedure was performed by PCR with Pfu DNA polymerase (Promega, Madison, WI, USA), followed by reverse transcription, degradation of RNA, and circularization with 5′-Full RACE Core Set (TaKaRa, Shiga, Japan) in the reaction mixture containing SD rat adult hippocampal RNA. Sequence analysis of the 5′-RACE products revealed that two different 5′-ends were present that are homologous to mouse full length MKL1 and BSAC, respectively. These two fragments were tentatively termed full-length MKL1 (FLMKL1) and basic, SAP and coiled-coil domain (BSAC), respectively. The predicted 1st and 2nd exons were absent in FLMKL1. Thus, the 5′-RACE was further performed with AmpliTaq Gold (Applied Biosystems, Carlsbad, CA, USA), 5′-Full RACE Core Set and primers (RT2: 5′-CCGCTCACTAAGTG-3′; sense3: 5′-GAACTGCAGGAGCTGTCCCT-3′; antisense3: 5′-TTGGCAACAGCTTCGCTCTG-3′; sense4: 5′-TGACTCTGGGCCTCCATCCT-3′; antisense4: 5′-CAGAGACAGGAGCACCGGTT-3′) corresponding to the predicted exon 3. The 5′-RACE product possesses a newly identified 5′-exon and was tentatively named MKL1-elongated derivative of yield (MELODY). To obtain FLMKL1, BSAC and MELODY cDNA including their coding regions, PCR was carried out with rat 7-week hippocampal cDNA as a template, PrimeSTAR Max DNA polymerase (TaKaRa), sense primers (5′-CGGTACCCGGGGATCCTCGCTAGCCACGCTCCCTC-3′ for FLMKL1; 5′-CGGTACCCGGGGATCGCTGGGCTTCCTGTCTGCAC-3′ for BSAC; 5′-CGGTACCCGGGGATCGCAGAGACACCTGTCAGGAC-3′ for MELODY) and antisense primer (5′-CGACTCTAGAGGATCGCCTCTAGGGACTGTGATTGTC-3′ for a common 3′-untranslated region). The sequence analyses of FLMKL1 (DDBJ Accession No. AB588919), BSAC (AB588920) and MELODY (AB588921) were deposited.

2.3. Search of transcription factor-binding sites within rat MKL1 genome

To find transcription factor-binding sites upstream of transcription start site of rat MKL1 isoforms, we used the TF search program (http://mbs.cbrc.jp/research/db/TFSEARCH.html), which is directly owned to the TRANSFAC databases developed at GBF-Braunschweig, Germany [13]. Rat MKL1 genome sequences, shown in the website of Ensembl database (http://www.ensembl.org/index.html), was used for TF search program. One kilobase long upstream of 5′-ends of FLMKL1, MELODY, BSAC were searched at threshold score = 95.0.

2.4. RNA isolation and real-time quantitative PCR

Total RNA was extracted from rat tissues and brain regions using TRIsure (Bioline). Then, RNA was treated with DNase I and further purified using TRIsure again. Using the RNA solution, cDNA was synthesized with SuperScriptII reverse transcriptase (Invitrogen, Carlsbad, CA, USA). In brief, for detection of FLMKL1, BSAC, and MELODY mRNA levels, the PCR was performed in 20 μL of 1 × SYBR system using SYBR Green PCR master mix (Applied Biosystems, Foster City, CA, USA) containing 2 μL of cDNA solution and 0.4 μM primers (5′-TCCTTGAGGCTCGGGAGGATA-3′ and 5′-GTCCAGCCCATTCACAGCAATG-3′ for FLMKL1; 5′-GCTTCCTGTCTGCACTCACTC-3′ and 5′-GACGGAGTCCTCACGGAAAC-3′ for BSAC; 5′-CAGAGACACCTGTCAGGACG-3′ and 5′-GTCCAGCCCATTCACAGCAATG-3′ for MELODY). After preheating at 95 °C for 10 min, the samples were denatured at 95 °C for 45 s, annealed at 60 °C for 45 s, and extended at 72 °C for 1 min for 45 cycles. Quantification of each transcript was calculated by the following procedure. In brief, the initial cDNA copy number [DNA_0], which reflects mRNA expression of the sample, was calculated from PCR-amplified cDNA copy number [DNA], Ct value (c), amplification efficiency (e) and cDNA standard curve. The formula, $[DNA] = [DNA_0](1 + e)^c$, was used for calculation.

2.5. Plasmids and antibodies

To generate a series of FLAG-tagged rat MKL1 constructs (FLAG-FLMKL1, FLAG-BSAC, FLAG-MELODY and FLAG-MKL1met), the coding regions of FLMKL1 (from 5′-CCCCCTTCCGTCATT-3′ to 5′-TGGGATTCCTGCTTG-3′), BSAC (from 5′-ACTCTGCTGGAGCCT-3′ to 5′-TGGGATTCCTGCTTG-3′), MELODY (from 5′-GGAGGGGTTACCATC-3′ to 5′-TGGGATTCCTGCTTG-3′) and MKL1met (from 5′-CCGCCTTTGAAAAGT-3′ to 5′-TGGGATTCCTGCTTG-3′) were linked to the downstream (5′-CTTGCGGCCGCGAATTCA-3′) of the FLAG tag sequence of pFLAG-CMV2 vector (SIGMA, St. Louis, MO, USA). The expression vector for enhanced green fluorescent protein (pEGFP-C1) was purchased from Clontech. The SRF reporter vector, 3D.ALuc, generously provided by Dr. R. Treisman (Cancer Research Institute, London, UK) has been described previously [6,9,11]. The CRE-reporter vector, pCRE-Luc (CRE-Luc), and the SRE-reporter vector, pSRE-Luc (SRE-Luc), were purchased from Stratagene (La Jolla, CA, USA). An internal control vector, TK-*Renilla* vector, has been described previously [9]. The following antibodies were used: anti-green fluorescent protein (GFP) made in rabbit (Invitrogen or Medical & Biological Laboratories; 1:500 or 1:1000), anti-FLAG (SIGMA; 1:1000) made in mouse, and anti-α-tubulin (SIGMA; 1:1000) made in mouse.

2.6. Cell culture

NIH3T3 cells were cultured in Dulbecco's modified Eagle medium (DMEM; Invitrogen) containing 10% fetal bovine serum (Invitrogen), 10% Nu-serum (BD Biosciences, San Jose, CA, USA), 2 mM glutamine (Invitrogen), 1% penicillin/streptomycin (Invitrogen), as described previously [9]. For reporter assays, cells were seeded at 5 × 10^5 cells/well and grown on six-well plates (Nalge Nunc, Naperville, IL, USA).

2.7. Transfection into NIH3T3 cells

Transfection into NIH3T3 cells was performed using lipofectamine (Invitrogen) and Plus reagent (Invitrogen) as described previously [9]. Medium exchange was carried out 4 h after transfection. Cell lysates were prepared 20 h after transfection.

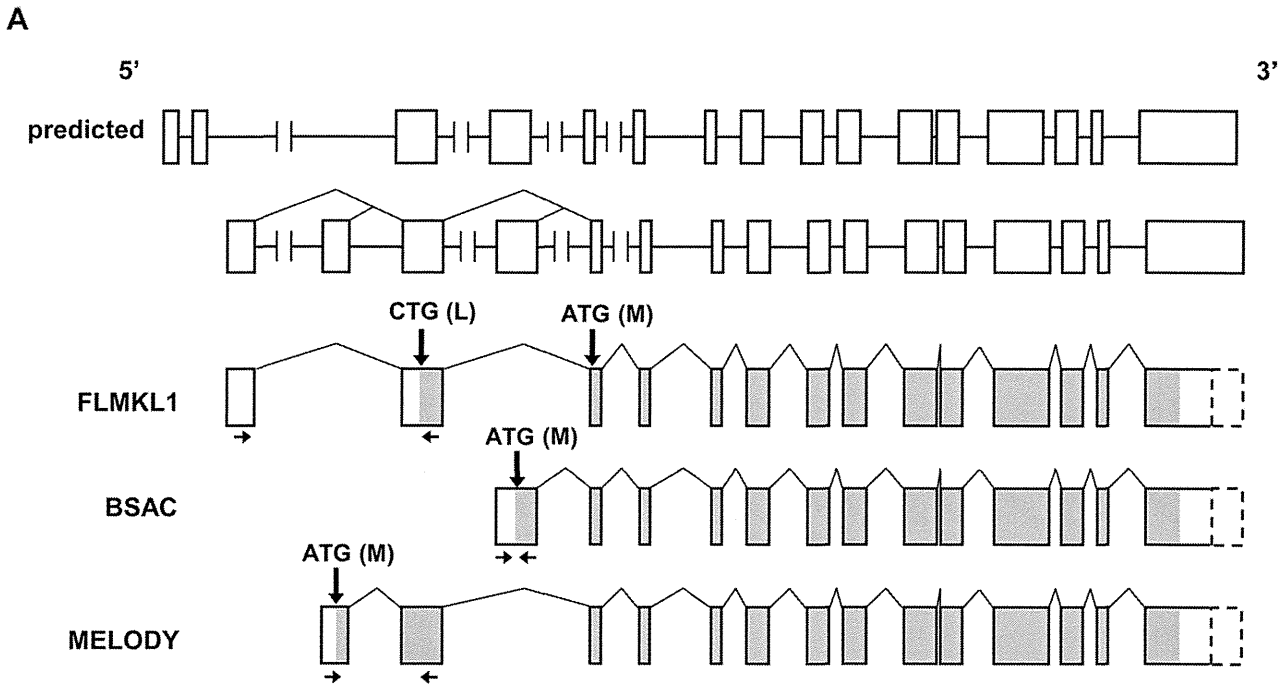

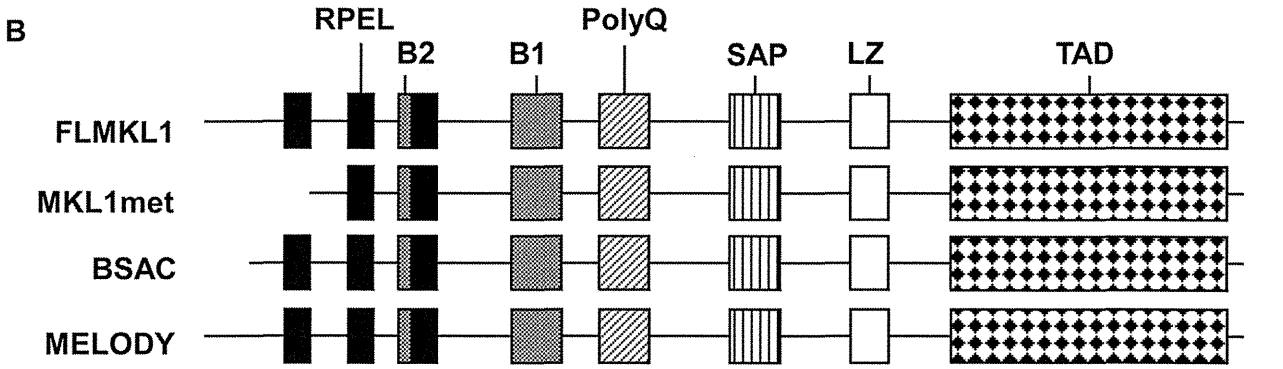

C

```
(FLMKL1)    1:------------------LPPSVIAVNGLDGGGAGENDEEPVLLSLSAAPSPQSEAVANELQELSLQPEL  52
(MKL1met)   0:------------------------------------------------------------------------  0
(BSAC)      0:------------------------------------------------------------------------  0
(MELODY)    1:MGGVTITKAKVDFSSVVCLPPSVIAVNGLDGGGAGENDEEPVLLSLSAAPSPQSEAVANELQELSLQPEL  70
                                                  RPEL
           53:TLGLHPGRNPNLPPLSERKNVLQLKLQQRRTREELVSQGIMPPLKSPAAFHEQRRSLERARTEDYLKRKI 122
            1:----------------------------------------MPPLKSPAAFHEQRRSLERARTEDYLKRKI  30
            1:-----MTLLEPEMLMMAVQSVLQLKLQQRRTREELVSQGIMPPLKSPAAFHEQRRSLERARTEDYLKRKI  65
           71:TLGLHPGRNPNLPPLSERKNVLQLKLQQRRTREELVSQGIMPPLKSPAAFHEQRRSLERARTEDYLKRKI 140
```

Fig. 1. Deduced exon–intron organization and domain structure of rat MKL1 isoforms. (A) Deduced exon–intron organization. Boxes indicate exons. Sizes of exons and introns are depicted approximately to scale. The predicted exon locations (on the top) are illustrated in accordance with the NCBI's information (NCBI Reference Sequence: XM_235497.4 and NW_047780.1). The exon (open boxes)–intron organization (the second from the top) is illustrated based on the sequence data shown in this study. The last three structures indicate the deduced exon–intron organization of FLMKL1, BSAC and MELODY variants, respectively. Shaded regions indicate the open reading frames. Boxes drawn by broken lines indicate the predicted 3′-untranslated regions, which were not analyzed in this study. Thick arrows indicate the putative initiation codons. Thin arrows indicate the location of primers used for real-time quantitative PCR measurements of each mRNA transcript. The FLMKL1 possesses two putative initiation codons, possibly giving rise to two different proteins, FLMKL1 and MKL1met, respectively (also shown in Fig. 1B). (B) Conserved motifs of FLMKL1, MKL1met, BSAC and MELODY. The illustrated domains were predicted on the basis of Pfam (http://www.sanger.ac.uk/). FLMKL1 and MKL1met can be produced by the distinct usage of two initiation codons, CTG and ATG, in a common transcript, respectively (see (A)). RPEL: arginine proline XXX glutamate leucine; B1 and B2: basic regions 1 and 2; PolyQ: polyglutamine repeat; SAP: SAF-A/B, Acinus and PIAS; LZ: leucine zipper; TAD: transcriptional activation domain. (C) Variation of the N-termini of FLMKL1, MKL1met, BSAC and MELODY. The numbers at both ends indicate the amino acid position of each isoform. The rectangle indicates the first RPEL motif. The first amino acids of the RPEL motif are written in white.

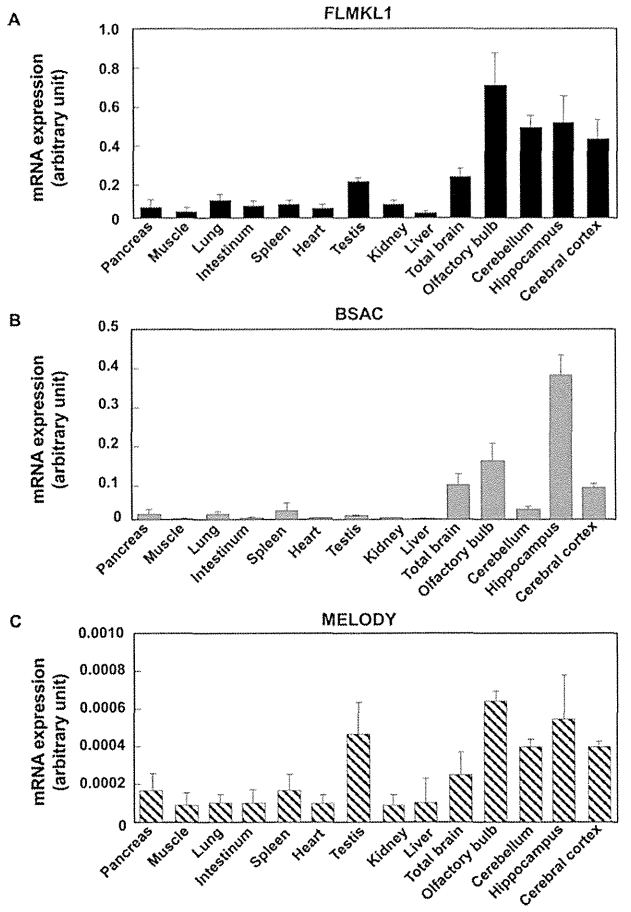

Fig. 2. Regional expression of rat MKL1 transcripts in adult tissues. Complementary DNA derived from several tissues of 7-week old rat (pancreas, muscle, lung, intestinum, spleen, heart, testis, kidney, liver, total brain, olfactory bulb, cerebellum, hippocampus and cerebral cortex) was subjected to real-time quantitative PCR analysis with FLMKL1 (A), BSAC (B), MELODY (C) specific primers. Primer positions are illustrated in Fig. 1A. Data represent the means ± SD from at least three independent experiments.

2.8. Western blotting

In order to measure the expression levels of FLAG-tagged rat MKL1 variants, we performed Western blotting for the FLAG tag (Fig. 4A). Protein was extracted in the whole cell extract buffer containing 25 mM HEPES, 0.3 M NaCl, 1.5 mM $MgCl_2$, 0.2 mM EDTA, 0.1% Triton X-100, 20 mM β-glycerophosphate, 10 μg/mL aprotinin, 10 μg/mL leupeptin, 1 mM sodium orthovanadate, 1 mM dithiothreitol, and 1 mM phenylmethylsulfonyl fluoride. After centrifugation, the cell lysates were mixed with an equal volume of 2 × Laemmli sample buffer (Bio-Rad Laboratories, Hercules, CA, USA) and subjected to sodium dodecyl sulfate–polyacrylamide gel electrophoresis. Protein detection was carried out with the enhanced chemiluminescence (ECL) protocol (GE Healthcare, Little Chalfont, UK).

2.9. Reporter assay

Transcriptional activity was monitored using either the firefly luciferase or *Renilla* luciferase activity as described previously [9]. Luciferase activity was monitored using dual luciferase assays according to the manufacturer's instructions (Promega).

2.10. Statistical analysis

Statistical significance of treatment effects was analyzed by ANOVA.

3. Results

3.1. Identification of rat MKL1 transcripts

To identify rat MKL1 transcripts, we first designed primers for 5′-rapid amplification cDNA-end (5′-RACE) based on the predicted rat MKL1 mRNA sequence (NCBI Reference Sequence: XM_235497.4) (Fig. 1A, on the top). Sequence analysis of the 5′-RACE products generated from primers located in predicted exons 7 and 8 revealed that two different 5′-ends were present that were homologous to mouse full length MAL/MKL1 and BSAC. However, since the predicted exons 1 and 2, which were provided by NCBI reference sequence, were absent from the presumed 5′ fragment of rat FLMKL1, we performed another round of 5′-RACE with primers corresponding to the predicted exon 3. Although these 5′-RACE products still did not contain sequences corresponding to either of the predicted exons 1 and 2, which were provided by NCBI reference sequence, they did contain a transcript with a novel 5′ exon that we refer to as MELODY (MKL1-elongated derivative of yield). Subsequent cloning and sequence analysis of the entire FLMKL1 (DDBJ: AB588919), BSAC (DDBJ: AB588920) and MELODY (DDBJ: AB588921) cDNAs revealed that the predicted 1st and 2nd exons were absent from all three rat MKL1 cDNA obtained in this study (Fig. 1A). Each of the three rat MKL1 transcripts identified have distinct 5′-exons, implying that alternative promoters may be located upstream of each of these 5′-exons. To find transcription factor-binding sites of rat MKL1 gene, we used TF search [13]. Binding sites of ETS, AML-1a are located within 1 kbp upstream of 5′ ends of FLMKL1. Binding sites of SRY, CdxA, Nkx-2 are located within 1 kbp upstream of 5′ ends of MELODY. SRY, CdxA are located within 1 kbp upstream of 5′ ends of BSAC cDNA. These binding sites may be involved in differential regulation of MKL1 isoform transcription.

The study by Miralles et al. demonstrated that mouse FLMKL1 contains two alternative translation start sites [6]. The two translation products generated, FLMKL1 and MKL1met, possess three and two RPEL motifs, respectively (Fig. 1B, on the top and the second rows). Although the junction between the distinct 5′ exon located in BSAC and the first exon shared in common by all the transcripts is located at the N-terminal border of the first RPEL domain, we noted that amino acid sequences of this domain is identical in BSAC, FLMKL1 and MELODY, except for the very first amino acid residue which is switched to serine in BSAC instead of asparagine present in FLMKL1 and MELODY (Fig. 1C). The nucleotide and amino acid sequences of rat MKL1 transcripts identified here are summarized in supporting information figures available online (Figs. S1, S2 and S3). In comparing these cDNA nucleotide sequences with the corresponding rat genomic sequence (NCBI Reference Sequence: NW_047780.1 and NW_001084859.1), we noted a discrepancy in one nucleotide (the 2816th base in FLMKL1 (DDBJ: AB588919), the 2671st base in BSAC (DDBJ: AB588920) and the 2798th base in MELODY (DDBJ: AB588921) (Figs. S1, S2 and S3). All three cDNA sequences contain T residues rather than a C residue reported in the genomic database, a substitution that would result in a switch from serine to leucine. It is still unknown whether or not this conversion is due to RNA editing or a single nucleotide polymorphism.

3.2. Tissue-distribution of rat MKL1 transcripts

We next examined the tissue-distribution of FLMKL1, BSAC, and MELODY mRNAs. Specific primers were designed for the detection of FLMKL1, BSAC and MELODY expression as shown in Fig. 1A (arrows). Initially, we confirmed whether quantitative PCR analysis could detect the mRNA expression of each transcript specifically. No PCR-amplification was observed in the reverse transcription-free samples (Fig. S4, control−), but bands appeared when each transcript-carrying plasmid template (Fig. S4, control+) or reverse transcribed samples (Fig. S4, 14 kinds of tissues) were used. This showed that PCR products

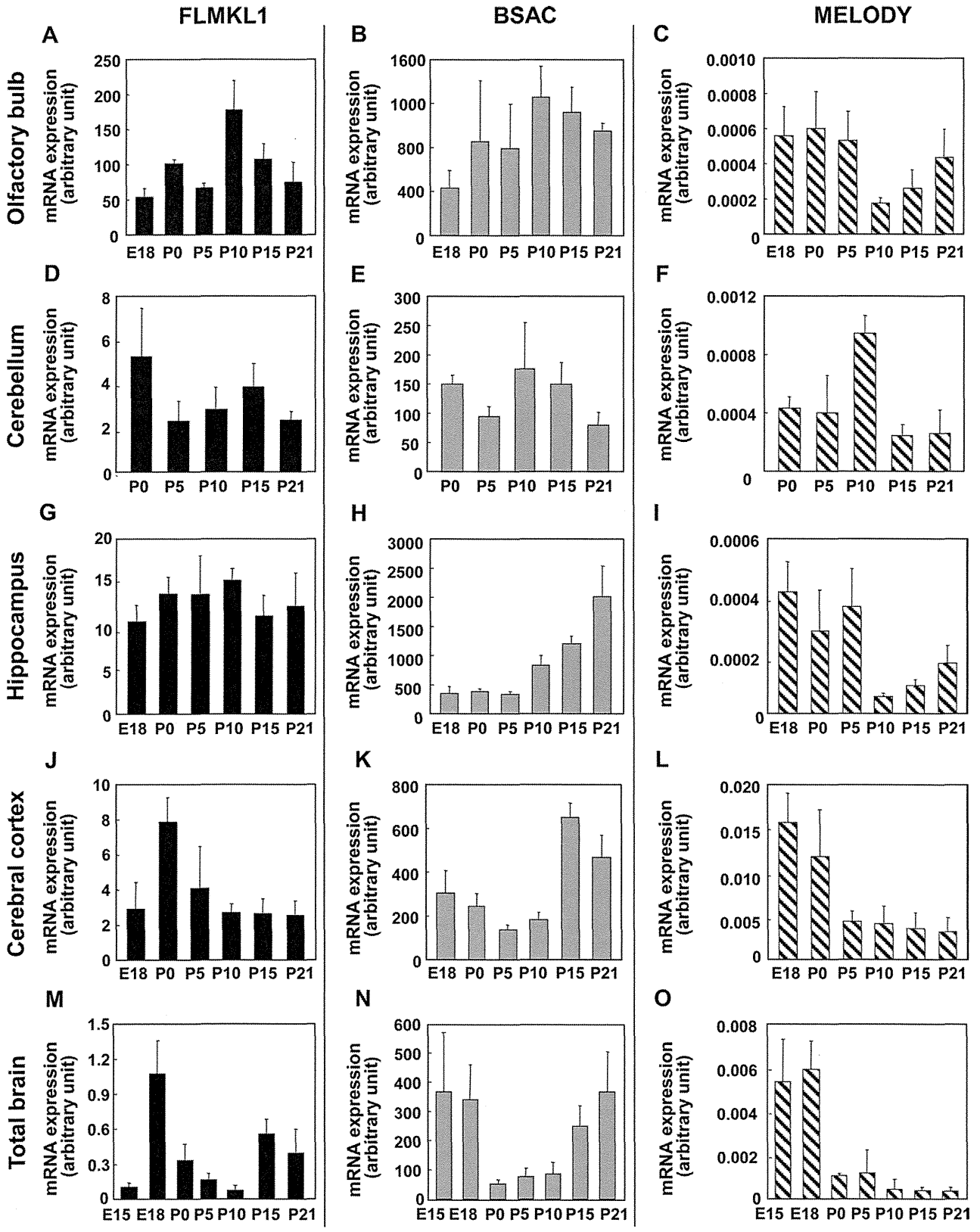

Fig. 3. Differential expression of rat MKL1 transcripts in the developing brain. Samples were prepared from the olfactory bulb (A–C), cerebellum (D–F), hippocampus (G–I), cerebral cortex (J–L) and total brain (M–O) and subjected to real-time quantitative PCR analysis with FLMKL1 (A, D, G, J and M), BSAC (B, E, H, K and N) and MELODY (C, F, I, L and O) specific primers. E15, embryonic day 15; E18, embryonic day 18; P0, post-natal day 0 (day of birth); P5, post-natal day 5; P10, post-natal day 10; P15, post-natal day 15, P21; post-natal day 21. Bar graphs represent the means ± SD from at least three independent experiments.

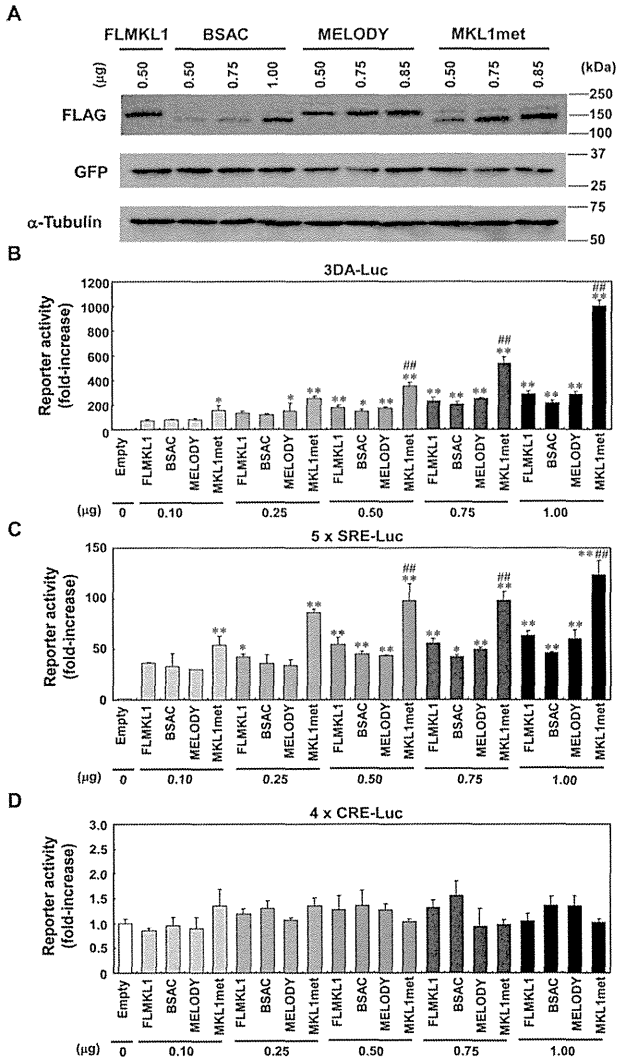

Fig. 4. Effects of MKL1 isoforms on SRF- and CREB-mediated transcriptional responses in NIH3T3 cells. (A) The expression level of FLAG-tagged MKL1 variants. FLAG-tagged FLMKL1, BSAC, MELODY or MKL1met (the amount indicated as 0.50–1.00) was co-transfected with GFP vector (1 μg/well) into NIH3T3 cells. Twenty-four hours later, cell lysates were collected and Western blotting was performed. In transfection studies presented in this and subsequent figures, empty vector was added as needed to keep the total amount of expression vectors used for transfection per well constant. (B–D) Either 1.0 μg/well of empty vector (Empty), 0.1, 0.25, 0.5, 0.75 and 1.0 μg/well of FLAG-tagged FLMKL1, BSAC, MELODY or MKL1met was co-transfected with firefly luciferase vector (B: 3D.A.Luc, C: 5 × SRE-Luc, D: 4 × CRE-Luc, 1.0 μg/well) and Renilla luciferase reporter vectors, TK-Renilla (0.2 μg/well) into NIH3T3 cells. Twenty-four hours later, luciferase activities were measured. To keep the total amount of transfected vector constant (2 μg total/well), empty vector was added as needed. Bar graphs represent the means ± SD from at least three samples. $^{*}p < 0.05$ (vs. empty), $^{**}p < 0.01$ (vs. empty), $^{***}p < 0.001$ (vs. empty), $^{\#\#}p < 0.01$ (vs. FLMKL1).

were derived from cDNA, but not from contamination with genomic DNA. Furthermore, only one band was generated in each assay and it had the predicted size, suggesting that the quantitative PCR analysis specifically detected only one amplified band of interest, but not non-specific bands. Two initiator codons of FLMKL1 give rise to two translation products, FLMKL1 and MKL1met. Therefore, the PCR products amplified with primers for FLMKL1 included both FLMKL1 and MKL1met. Quantitative real-time PCR revealed that all MKL1 transcripts were enriched in the nervous system (Fig. 2) and that the level of MELODY mRNA was very low compared to other transcripts (Fig. 2C). As expression of MELODY is orders of magnitude below that of FLMKL1 and BSAC, its impact on cell signaling is unclear. The expression of FLMKL1 and MELODY was relatively high in the testis and the olfactory bulb (Fig. 2A and C). BSAC was enriched in the hippocampus (Fig. 2B).

3.3. Developmental regulation of rat MKL1 transcripts in the brain

As the tissue survey described above showed that MKL1 mRNA was highly expressed in the brain (Fig. 2), we proceeded to determine the expression profile of MKL1 transcripts during brain development. Using quantitative PCR analysis of cDNAs derived from several brain regions at different developmental stages, we found that BSAC was the most abundant of the three MKL1 transcripts during brain development (Fig. 3). The expression level of BSAC mRNA increased after P10–P15 in both the hippocampus and the cerebral cortex (Fig. 3H and K). In contrast, MELODY mRNA level decreased during development in several brain regions (Fig. 3C, I, L and O). The expression pattern of FLMKL1 mRNA during development varied across different regions (Fig. 3A, D, G, J and M). In combination, these data show that the pattern of expression of the alternative transcripts generated from the rat MKL1 gene is dynamically regulated during brain development.

3.4. SRF coactivator function of rat MKL1 isoforms

Next, we examined the functional activities of MKL1 isoforms in NIH3T3 cells. We first checked the expression level of FLAG-tagged MKL1 isoforms. As shown in Fig. 4A, the expression levels of MKL1 isoforms were varied when 0.50–1.00 μg of FLAG-MKL1 expression vectors were transfected. Likewise, we also checked the effects of these four MKL1 isoforms on SRF-mediated transcriptional responses in NIH3T3 cells. All four MKL1 isoforms increased SRF-mediated transcriptional responses (Fig. 4B and C). When the same amounts of MKL1 expression vector were transfected into NIH3T3 cells, MKL1met was the most effective in driving SRF-mediated transcription among the four MKL1 isoforms. On the other hand, all four MKL1 isoforms did not activate cAMP response element (CRE)-mediated transcription significantly in NIH3T3 cells (Fig. 4D).

4. Discussion

In this study, we have identified three transcripts generated from the rat MKL1 gene: two of these, FLMKL1 and BSAC are homologous to mouse MKL1 transcripts, while the third, MELODY, represents a novel transcript (Fig. 1). Analysis of the exon–intron structure of these transcripts demonstrated that each has a distinct 5′-exon, implying that their transcription may be regulated separately by alternative promoters. Searching transcription factor-binding sites revealed that candidate binding sites of transcription factors located upstream of 5′-ends of rat MKL1 isoforms were different. This indicates that different transcription factors may be involved in the transcription of MKL1 isoforms in a spatiotemporal manner. In fact, analysis of their expression profiles revealed that all three MKL1 transcripts are enriched in the nervous system and display distinct spatiotemporal patterns of expression during brain development (Figs. 2 and 3). In terms of expression levels, there was a marked difference among the three MKL1 transcripts; in particular, the expression of MELODY is substantially lower than the other two transcripts (Figs. 2 and 3). Therefore, the influence of endogenous MELODY on SRF-mediated transcription under basal conditions may be negligible.

The functional properties of rat MKL1 isoforms indicates that the novel MKL1 isoform, MELODY, in addition to rat FLMKL1, BSAC, MKL1met isoforms strongly enhanced SRF coactivation (Fig. 4B and C). Analysis of the domain structure of the proteins generated from these MKL1 transcripts indicate that FLMKL1, BSAC and MELODY have three G-actin-binding RPEL motifs, while MKL1met has two RPEL motifs (Fig. 1). Comparison in every amount of MKL1 isoform vectors showed that MKL1met tends to be more active than other isoforms. Three RPEL motifs in a single MKL1 molecule appear to bind

to five G-actins [14]. Assuming that loss of one of these RPEL motifs decreases the stoichiometry and/or affinity of the interaction of MKL1 met with G-actin, may promote the nuclear localization, and may cause stronger activity of SRF coactivator function. In this study, we evaluated the effect of overexpressed MKL1 isoforms in NIH3T3 cells. Thus, further studies would be required for identification and function of endogenous MKL1met protein in a variety of cell types and tissues.

Although we have identified rat MKL1 isoforms, it is important to note that additional MKL1 isoforms may remain to be identified. Stern et al. [15] indicate that an MAL/MKL1 variant of relatively small size (approximately 65 kDa) is expressed in neurons. Since the rat MKL1 variants identified in this study are much larger, this smaller variant may represent another rat MKL1 variant that remains to be characterized. Further studies are needed to determine if this putative ~65 kDa form is generated from a distinct transcript or via alternative translation of one of the three transcripts described herein.

Analysis of another SRF coactivator, myocardin, [16] has demonstrated that alternative splicing gives rise to myocardin protein isoforms with different N-termini, a region that contains RPEL motifs [17]. Notably, differences in this N-terminal region affect binding of myocardin to myocyte enhancer factor 2 (MEF2), thereby regulating MEF2-mediated transcription [17]. In a similar vein, it is conceivable that the different N-termini found in MKL1 isoforms may also mediate their differential interaction with other transcription factors. To clarify the functional role of the distinct N-terminal regions of MKL1 isoforms, further studies aimed at searching for interacting proteins or at examining isoform-specific knock down by RNA interference may be valuable.

In summary, we have identified a set of rat MKL1 transcripts that are differentially expressed in developing and mature brain. Our previous study demonstrated that SRF-target β-actin gene promoter was increased by overexpression of mouse MKL1 and MKL2 in primary cultured cortical neurons [12]. To precisely investigate differential effects of MKL1 isoforms on endogenous SRF-target genes, the rescue experiments with overexpression of MKL1 isoforms in the cells, derived from MKL1 knock-out mice, might be needed. Taken together, our findings suggest that expression of multiple MKL1 isoforms helps to fine tune changes in gene expression in both developing and mature brain.

Conflict of interest

The authors have no competing financial interest or further conflict of interest.

Acknowledgements

This study was supported by a grant-in aid from the Ministry of Education, Culture, Sports, Science and Technology of Japan (Project No. 17790055, 19790052 and 22590080, A.T.; 20390023, M.T.; 23890065, M.I.) and by research grants from the Hayashi Memorial Foundation for Female Natural Scientists (A.T.), Foundation of the first Bank of Toyama (A.T.), Takeda Science Foundation (A.T.), Narishige Neuroscience Research Foundation (A.T.) and the Research Foundation for Pharmaceutical Sciences (A.T.).

Supplementary material

Supplementary material associated with this article can be found, in the online version, at doi:10.1016/j.fob.2013.09.001.

References

[1] Wang, D.Z., Li, S., Hockmeyer, D., Sutherland, L., Wang, Z., Schratt, G. et al. (2002) Potentiation of serum response factor activity by a family of myocardin-related transcription factors. Proc. Nat. Acad. Sci. USA 99, 14855–14860.
[2] Sasazuki, T., Sawada, T., Sakon, S., Kitamura, T., Kishi, T., Okazaki, T. et al. (2002) Identification of a novel transcriptional activator, BSAC, by a functional cloning to inhibit tumor necrosis factor-induced cell death. J. Biol. Chem. 277, 28853–28860.
[3] Selvaraj, A. and Prywes, R. (2003) Megakaryoblastic leukemia-1/2, a transcriptional co-activator of serum response factor, is required for skeletal myogenic differentiation. J. Biol. Chem. 278, 41977–41987.
[4] Cen, B., Salvaraj, A. and Prywes, R. (2004) Myocardin/MKL family of SRF coactivator: key regulators of immediate early and muscle specific gene expression. J. Cell Biochem. 93, 74–82.
[5] Pipes, G.C., Creemers, E.E. and Olson, E.N. (2006) The myocardin family of transcriptional coactivators: versatile regulators of cell growth, migration and myogenesis. Genes Dev. 20, 1545–1556.
[6] Miralles, F., Posern, G., Zaromytidou, A.I. and Treisman, R. (2003) Actin dynamics control SRF activity by regulation of its coactivator MAL. Cell 113, 329–342.
[7] Posern, G., Miralles, F., Guettler, S. and Treisman, R. (2004) Mutant actins that stabilize F-actin use distinct mechamisms to activate the SRF coactivator MAL. Embo J 23, 3973–3983.
[8] Vartiainen, M.K., Guettler, S., Larijani, B. and Treisman, R. (2007) Nuclear actin regulates dynamis subcellular localization and activity of the SRF cofactor MAL. Science 316, 1749–1752.
[9] Tabuchi, A., Estevez, M., Henderson, J.A., Marx, R., Shiota, J., Nakano, H. et al. (2005) Nuclear translocation of the SRF co-activator MAL in cortical neurons: role of RhoA signaling. J. Neurochem. 94, 169–180.
[10] Kalita, K., Kharebava, G., Zheng, J.J. and Hetman, M. (2006) Role of Megakaryoblastic acute leukemia-1 in ERK1/2-dependent stimulation of serum response factor-driven transcription by BDNF or increased synaptic activity. J. Neurosci. 26, 10020–10032.
[11] Shiota, J., Ishikawa, M., Sakagami, H., Tsuda, M., Baraban, J.M. and Tabuchi, A. (2006) Developmental expression of the SRF co-activator MAL in brain: role in regulating dendritic morphology. J. Neurochem. 98, 1778–1788.
[12] Ishikawa, M., Nishijima, N., Shiota, J., Sakagami, H., Tsuchida, K., Mizukoshi, M. et al. (2010) Involvement of the SRF coactivator megakaryoblastic leukemia in the activin-regulated dendritic complexity of rat cortical neurons. J. Biol. Chem. 285, 32734–32743.
[13] Heinemeyer, T., Wingender, E., Reuter, I., Hermjakob, H., Kel, A.E., Kel, O.V. et al. (1998) Databases on transcriptional regulation: TRANSFAC, TRRD, and COMPEL. Nucleic Acids Res. 26, 364–370.
[14] Mouilleron, S., Langer, C.A., Guettler, S., McDonald, N.Q. and Treisman, R. (2011) Structure of a pentavalent G-actin MRTF-A complex reveals how G-actin controls nucleocytoplasmic shuttling of a transcriptional coactivator. Sci. Signal 4, ra40 .
[15] Stern, S., Debre, E., Stritt, C., Berger, J., Posern, G. and Knöll, B. (2009) A nuclear actin function regulates neuronal motility by serum response factor-dependent gene transcription. J. Neurosci 29, 4512–4518.
[16] Wang, D., Chang, P.S., Wang, Z., Sutherland, L., Richardson, J.A., Small, E. et al. (2001) Activation of cardiac gene expression by myocardin, a transcriptional cofactor fro serum response factor. Cell 105, 851–862.
[17] Creemers, E.E., Sutherland, L.B., Oh, J., Barbosa, A.C. and Olson, E.N. (2006) Coactivation of MEF2 by the SAP domain proteins myocardin and MASTR. Mol. Cell 23, 83–96.